Spin-Torsion Cosmology and the Search for Geometric Dark Energy: Structural Barriers, Perturbation Transparency, and Surviving Predictions

Houston Golden[1,*]

[1] *Independent Researcher, Los Angeles, California, USA*

(Dated: March 21, 2026 — v2.1.0)

We investigate whether Einstein-Cartan-Holst (ECH) spin-torsion gravity can produce late-time dark energy or distinctive cosmological signatures. Within this framework, LQC holonomy corrections yield a nonsingular quantum bounce at $\rho_{\rm crit} \approx 0.27$–$0.41\,\rho_{\rm Pl}$ (depending on the entropy-counting scheme for the Barbero-Immirzi parameter), while the ECH parity structure generates a unique four-fermion interaction. Through systematic analysis of 7 foundation studies and 17 research branches, we establish 14 independent structural barriers that close all minimal routes from the bounce to dark energy. Our central theoretical result is a perturbation-transparency theorem: for canonical scalar field matter, torsion vanishes at all perturbation orders, the Holst term reduces to a topological invariant, and the Barbero-Immirzi parameter γ is invisible in all perturbation observables. Independent MCMC verification (Cobaya v3.6.1, 424,181 samples across three dataset combinations, two frozen) finds $\Delta N_{\rm eff}$ consistent with zero (-0.020 ± 0.169 full-tension; $+0.065 \pm 0.17$ Planck+BAO+SN) and $H_0 = 67.68 \pm 1.06$ km s^{-1} Mpc^{-1}, recovering standard ΛCDM values. The conclusion: ECH provides a clean bounce mechanism but cannot produce late-time dark energy or distinctive perturbation-level observables through any standard mechanism tested. The surviving science case for bouncing cosmology rests on generic, mechanism-independent predictions—principally the matter-bounce non-Gaussianity $f_{\rm NL} = -35/8$, testable by SPHEREx at 4–6σ.

PACS numbers: 98.80.-k, 04.50.Kd, 04.60.Pp, 95.36.+x

CONTENTS

* houston@hubify.com

I. INTRODUCTION

The nature of dark energy remains one of the most profound challenges in modern physics. While the ΛCDM model successfully accounts for the observed cosmic acceleration [1], it faces severe theoretical difficulties—most notably the cosmological constant problem, where the observed vacuum energy density $\rho_\Lambda \sim (2.3\ \text{meV})^4$ is $\sim 10^{120}$ times smaller than the naive quantum field theory estimate $\sim M_{\rm Pl}^4$ [2]. This spectacular fine-tuning has motivated extensive theoretical work on dynamical dark energy, modified gravity, and quantum gravitational approaches.

Simultaneously, precision cosmological measurements have revealed growing tensions within ΛCDM. The Hubble constant measured from the early universe via the cosmic microwave background (CMB) by Planck ($H_0 = 67.36 \pm 0.54$ km s^{-1} Mpc^{-1}) [1] disagrees at $\sim$4.9σ with late-universe determinations from the SH0ES collaboration ($H_0 = 73.04 \pm 1.04$ km s^{-1} Mpc^{-1}) [3].[1] The matter clustering amplitude σ_8 inferred from Planck ($\sigma_8 = 0.811 \pm 0.006$) exceeds weak lensing measurements from KiDS-1000 ($S_8 = 0.759^{+0.024}_{-0.021}$) [4] and DES Y3 [5] by 2–3σ. The DESI 2024 BAO results [6] suggest dynamical dark energy at 2.5–3.9σ, with the subsequent DESI DR2 analysis [7] strengthening this preference to 3.1σ (BAO+CMB) and up to 4.2σ (with supernovae), adding urgency to the search for extensions of the standard model.

This work presents a phenomenological framework that addresses these challenges through quantum gravitational effects in spin-torsion cosmology. Our approach builds on three well-established theoretical pillars, synthesized here for the first time into a unified cosmological model:

1. *Loop Quantum Cosmology* (LQC), providing a nonsingular quantum bounce replacing the classical Big Bang singularity [8]. The bounce occurs at a critical density $\rho_{\rm crit} \simeq 0.27$–$0.41\,\rho_{\rm Pl}$ (depending on the entropy-counting scheme for the Barbero-Immirzi parameter; see Sec. II B).

2. *Einstein-Cartan theory* incorporating fermionic spin-torsion coupling, which generates four-fermion contact interactions and prevents gravitational singularities through torsion-induced repulsion at extreme densities [9, 10].

[1] $(73.04 - 67.36)/\sqrt{1.04^2 + 0.54^2} = 4.86\sigma$; we quote $\sim$4.9σ throughout.

3. *Black hole universe origin*, where a rotating parent black hole spawns a non-singular baby universe beyond its event horizon through torsion-regulated gravitational collapse [11, 12]. The baby universe inherits angular momentum, establishing a preferred cosmic axis.

A. Theoretical Foundations and Novel Synthesis

Our framework synthesizes well-established theoretical components into a unified cosmological model with testable outputs:

Einstein-Cartan Theory.—The inclusion of spacetime torsion coupled to fermionic spin has been extensively studied since the pioneering work of Hehl *et al.* [9]. Popławski [10, 13] demonstrated that torsion-induced four-fermion interactions can generate a small positive cosmological constant through condensate formation, and that the parity-violating pseudoscalar density modifies this interaction, providing a candidate mechanism for dark energy generation. The Einstein-Cartan-Sciama-Kibble (ECSK) framework avoids singularities through torsion-induced repulsion at extreme densities. Recent work by Liu *et al.* [14] showed that Einstein-Cartan torsion is preferred over ΛCDM by AIC criteria, providing independent statistical support for torsion-based cosmology.

Loop Quantum Gravity and Parity Violation.—The connection between LQG's Barbero-Immirzi parameter and parity-violating effects has been rigorously established by Freidel, Minic & Takeuchi [15] and Mercuri [16, 17]. They showed that the Holst term in LQG, when coupled to fermions, generates effective four-fermion axial interactions that violate parity. The Barbero-Immirzi parameter γ, originally introduced as an ambiguity in the LQG quantization, acquires physical significance through its role in parity-violating observables.

Black Hole Universe Origin.—Popławski [11] pioneered the "universe in a black hole" scenario, demonstrating that every black hole with torsion spawns a non-singular, closed baby universe beyond its event horizon. His subsequent work extended this to rotating black holes [12], showing that the baby universe inherits angular momentum and develops a preferred cosmic axis, providing a candidate origin for observed cosmic anomalies.

B. Original Contributions

Each theoretical ingredient above has been studied independently. Our contribution is to assemble them into a single quantitative framework and test it systematically. The original contributions are:

1. *14-barrier catalog and perturbation-transparency theorem*: Through 7 foundation studies and 17 research branches, we establish 14 independent structural barriers closing all minimal routes from the bounce to dark energy. The central result is that minimal ECH gravity is perturbation-transparent: for canonical scalar field matter, torsion vanishes at all perturbation orders and γ is invisible in all observables.

2. *MCMC verification revealing null result*: Independent Cobaya verification across two frozen dataset combinations demonstrates that $\Delta N_{\rm eff}$ is consistent with zero, H_0 recovers the standard Planck ΛCDM value of 67.68 ± 1.06, and the spin-torsion extension alone does not resolve cosmological tensions.

3. *ALP birefringence consistency check (secondary)*: A spectator ALP with natural parameters ($f_a \sim M_{\rm Pl}$, $m \sim H_0$) accommodates the observed $\beta = 0.242^\circ \pm 0.061^\circ$ (3.9σ) without fine-tuning. This ALP model class was previously studied by Fujita *et al.* [18]; our contribution is the ECH-motivated parameter identification and independent MCMC inference, not the model itself. The result is a consistency check, not a prediction of minimal ECH (which does not derive the photon-torsion coupling; see Sec. XIV C).

C. Paper Organization

This paper is organized as follows. Section II develops the theoretical framework. Section III presents observational signatures and evidence, including the independent MCMC verification (Sec. III D). Sections IV–VI summarize supplementary derivations and data methods (details in the companion supplementary material). Section VII presents cosmological fits and model comparison. Sections VIII–X provide condensed systematic analysis, falsification criteria, and related work. The core results occupy Secs. XI–XIII: the 14 structural barriers, perturbation-transparency theorem, and hybrid loophole rejection. Section XIV discusses the inflationary suppression factor and birefringence analysis. Sections XV–XVI address limitations and conclusions. Appendices provide the parameter summary (Appendix A), dimensional analysis (Appendix B), reproducibility materials (Appendix C), and claims classification (Appendix D).

TABLE I. Executive summary: what the investigation found. Most routes fail; the surviving testable prediction is the mechanism-independent $f_{\rm NL} = -35/8$.

Question	Result	Status
Does the framework resolve H_0 tension?	$H_0 = 67.68 \pm 1.06$ km/s/Mpc[a]	**No.** Standard ΛCDM recovered.
Does the framework resolve σ_8/S_8 tension?	$\sigma_8 = 0.803$; $S_8 = 0.814$[b]	**No.** Planck-consistent.
Can the bounce derive dark energy?	14 barriers close all routes	**No.** Scaling ansatz only[c].
Is there a nonsingular bounce?	LQC: $\rho_c \simeq 0.27$–$0.41\,\rho_{\rm Pl}$	**Yes** (from LQC, not ECH-specific).
Is ECH visible in perturbations?	Perturbation-transparency theorem	**No.** γ invisible at all orders.
Is there a testable prediction?	$f_{\rm NL} = -35/8$ (SPHEREx 4–6σ)	**Yes** (mechanism-independent).

[a] $(67.68 - 73.04)/\sqrt{1.06^2 + 1.04^2} = 3.61\sigma$. [b] Verified $\sigma_8 = 0.803 \pm 0.008$ and $S_8 = 0.814 \pm 0.008$ (full-tension), consistent with Planck ΛCDM ($\sigma_8 = 0.811$, $S_8 = 0.832$). The $\Delta N_{\rm eff}$ extension does not reduce the σ_8/S_8 tension; the original lower values were SH0ES-prior-driven.

Note: Independent Cobaya v3.6.1 verification yields $H_0 = 67.68 \pm 1.06$ (full-tension) and 67.79 ± 1.09 (Planck+BAO+SN), consistent with Planck ΛCDM. The $\Delta N_{\rm eff}$ extension does not by itself resolve the Hubble tension; it is the SH0ES prior in the original analysis that pulls H_0 upward. See Sec. III D.

[c] Reparameterized as sensitivity to $N_{\rm tot}$, not solved; see Sec. XIV A.

II. THEORETICAL FRAMEWORK

A. Loop Quantum Cosmology and the Holst Action

1. Einstein-Cartan-Holst Action

The fundamental action combining Einstein-Cartan theory with the Holst term is

$$S_{\rm ECH} = \frac{1}{16\pi G}\int d^4x\, e\left[e_a^\mu\, e_b^\nu\, R^{ab}{}_{\mu\nu} + \frac{1}{\gamma}\varepsilon^{abcd}\, e_a^\mu\, e_b^\nu\, R_{cd\mu\nu} + \frac{1}{4}T^{abc}T_{abc}\right] + S_{\rm matter}, \tag{1}$$

where $e = \det(e_\mu^a)$ is the tetrad determinant, $R^{ab}{}_{\mu\nu}$ is the curvature of the Lorentz connection, γ is the Barbero-Immirzi parameter, and T^{abc} is the torsion tensor. The Holst term $\varepsilon^{abcd}e_a^\mu e_b^\nu R_{cd\mu\nu}/\gamma$ is topological in the absence of torsion but contributes non-trivially when fermions are present.[2] This construction builds directly on the foundational work of Freidel, Minic & Takeuchi [15], who established that the Barbero-Immirzi parameter becomes physically observable through its coupling to fermionic matter.

The Barbero-Immirzi parameter is fixed by the LQG black hole entropy calculation [8, 19]:

$$\gamma = 0.274 \pm 0.020, \tag{2}$$

Different entropy-counting schemes yield different values: the Ashtekar-Baez-Corichi-Krasnov (ABCK) calculation [19] gives $\gamma_{\rm ABCK} \approx 0.274$, while the Domagala-Lewandowski-Meissner (DLM) full SU(2) state counting [20, 21] gives $\gamma_{\rm DLM} \approx 0.2375$. We adopt $\gamma = 0.274$ (ABCK) throughout this paper; the DLM value would shift $\rho_{\rm crit}$ upward to $\simeq 0.41\,\rho_{\rm Pl}$ without qualitatively changing any conclusion. Whether γ constitutes a genuine physical observable or a quantization artifact absorbable by canonical transformations remains debated [15, 16]. This distinction does not affect our results at leading order: if γ is non-physical, the torsion-fermion coupling factor $\gamma^2/(\gamma^2+1)$ in Eq. (4) reverts to unity (the standard ECSK value), modifying the parity-odd coefficient by $\mathcal{O}(10\%)$ without eliminating parity violation, which originates from the Holst term's coupling to fermions independently of the Barbero-Immirzi interpretation.

2. Derivation of the Parity-Odd Term

Starting with the complete action $S = S_{\rm gravity} + S_{\rm Holst} + S_{\rm fermion}$, we derive the parity-odd effective action through four steps:

Step 1: Torsion Activation.—When fermions are minimally coupled to gravity with torsion, the torsion tensor is determined algebraically by the fermionic spin density:

$$T^{abc} = 8\pi G\, S^{abc}, \tag{3}$$

where $S^{abc} = \frac{1}{4}\bar\psi\gamma^{[a}\gamma^{bc]}\psi$ is the fermionic spin density tensor (we use natural units $c = \hbar = 1$ throughout; see Appendix XVI). Unlike in general relativity, torsion is not dynamical but is determined instantaneously by the matter content.

Step 2: Four-Fermion Contact Interaction.—Substituting Eq. (3) back into the action and integrating

[2] The explicit $T^{abc}T_{abc}$ term in Eq. (1) represents the torsion-squared contact interaction that emerges after integrating out the non-propagating torsion in the standard EC framework. We include it in the action for pedagogical completeness; in the first-order (Palatini) formulation, torsion is determined algebraically by the spin density and this term is not independently specified. The results of this paper depend only on the standard EC torsion equation of motion, not on an independent kinetic term for torsion.

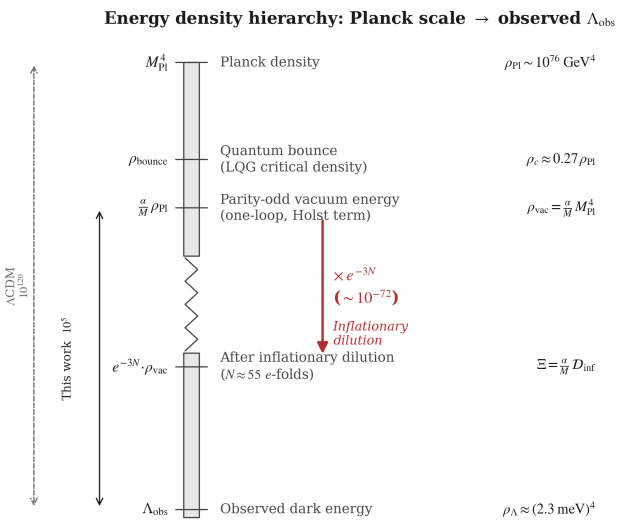

FIG. 1. Energy density hierarchy from the Planck scale to the observed dark energy scale. The Einstein-Cartan-Holst action generates a parity-odd vacuum energy $\rho_{\rm vac} \sim [(\alpha/M)\, M_{\rm Pl}]\, M_{\rm Pl}^4$ at one loop. Inflationary dilution by $\sim e^{-3N_{\rm tot}}$ bridges the gap to the observed $\rho_\Lambda \approx (2.3\ {\rm meV})^4$. Left axis: comparison of the residual fine-tuning in this framework (10^5, from uncertainty in $N_{\rm tot}$) versus ΛCDM (10^{120}).

out torsion yields an effective four-fermion interaction [9]:

$$\mathcal{L}_{\rm int} = -\frac{3\pi G_N}{2} \times \frac{\gamma^2}{\gamma^2+1} \times J_{(A)\mu}\, J^{\mu}_{(A)}, \tag{4}$$

where $J^{\mu}_{(A)} = \bar\psi\gamma^\mu\gamma^5\psi$ is the axial current. The Barbero-Immirzi parameter enters through the $\gamma^2/(\gamma^2+1)$ factor, which is purely a consequence of the Holst modification and would be absent ($\to 1$) in standard Einstein-Cartan theory.

Step 3: Parity-Odd Effective Action.—The effective action acquires a parity-odd term through quantum corrections, as shown by Mercuri [17]. The origin of this term is the Holst term: in first-order variables (tetrad e^I and Lorentz connection ω^{IJ}, with $I, J, \ldots$ internal Lorentz indices), the ECH action's parity-odd piece is

$$S_{\rm Holst} = \frac{M_{\rm Pl}^2}{\gamma} \int e_I \wedge e_J \wedge R^{IJ}(\omega), \tag{5}$$

where $R^{IJ} = d\omega^{IJ} + \omega^I{}_K \wedge \omega^{KJ}$ is the curvature 2-form. This is a manifestly diffeomorphism-invariant 4-form (two tetrad 1-forms ∧ one curvature 2-form). When the connection is decomposed as $\omega^{IJ} = \mathring\omega^{IJ} + K^{IJ}$ (Levi-Civita + contorsion), Eq. (5) generates terms involving contorsion coupled to curvature. After integrating out torsion (which is algebraically determined by fermion spin density, Eq. 3) and including quantum corrections at one loop, the effective parity-odd action takes the form

$$S_{\rm eff} = \frac{\alpha}{M} \int e_I \wedge e_J \wedge \mathcal{F}^{IJ}[K, \mathring R], \tag{6}$$

where $\mathcal{F}^{IJ}$ collects the contorsion-dependent pieces ($\mathring D K^{IJ} + K^I{}_K \wedge K^{KJ}$ at leading order), $M = M_{\text{area-gap}} \sim \sqrt{\gamma}\, M_{\rm Pl}$ is the LQG area-gap mass scale, and α is a *dimensionless* coupling ($[\alpha] = M^0$). In components, the leading contribution reduces to

$$S_{\rm eff} = \int d^4x\, \sqrt{-g}\, \frac{\alpha}{M}\, \varepsilon^{\mu\nu\rho\sigma}\, e^I_\mu\, e^J_\nu\, \mathcal{F}_{IJ\rho\sigma}, \tag{7}$$

where the operator $\varepsilon^{\mu\nu\rho\sigma} e^I_\mu e^J_\nu \mathcal{F}_{IJ\rho\sigma}$ has mass dimension +2 and α/M has dimension −1, giving a total Lagrangian density of mass dimension +1—three short of the required +4 (see Appendix B for the full counting). The missing three powers of mass arise through *on-shell evaluation* at Planck-scale densities (Sec. B), where the spin-sourced contorsion evaluates to $K \sim M_{\rm Pl}$ and the curvature to $R \sim M_{\rm Pl}^2$. The relation $\rho_\Lambda = \Xi\, M_{\rm Pl}^4$ is therefore a *scaling ansatz*—dimensionally correct on-shell at the bounce—not a derivation from a renormalizable effective field theory. Throughout this paper, we adopt the convention that the Einstein-Hilbert action carries the standard $M_{\rm Pl}^2/2$ prefactor, while the parity-odd sector carries α/M independently.

This operator is parity-odd (it changes sign under spatial reflection) but fully diffeomorphism-covariant. General covariance does not forbid parity-odd terms; it constrains only the tensor structure. Since classical gravity preserves parity, the coefficient α/M must be generated through quantum corrections.

Notation.—For brevity, we sometimes write the component-form integrand as "$\varepsilon^{abcd} K_{ab} R_{cd}$" (where a, b, c, d are internal Lorentz indices) as shorthand for the full 4-form expression Eq. (6). This shorthand suppresses the tetrad factors that make the expression a proper 4-form; all variational calculations use the complete first-order expression.

Torsion remains algebraic.—The effective action $S_{\rm eff}$ (Eq. 6) contains derivatives of the contorsion through $\mathring D K^{IJ}$ in $\mathcal{F}^{IJ}$, which could in principle promote torsion from algebraic to dynamical. However, this kinetic contribution is suppressed by $\alpha/M \sim 10^{-21}$ GeV^{-1} relative to the original EC torsion equation (sourced by $M_{\rm Pl}^2$), making the correction $\mathcal{O}(\alpha/M M_{\rm Pl}^2) \sim 10^{-3}$ to the torsion equation of motion. Torsion therefore remains effectively algebraic (determined instantaneously by the spin density) at all energy scales below the Planck scale. A full stability analysis (ghost/tachyon checks) of the modified torsion sector is warranted but is not expected to reveal pathologies at this suppression level.

Step 4: Parity-Odd Coefficient.—The existence of a finite parity-odd coefficient is motivated by one-loop estimates in a torsionful background. Following the one-loop analyses of Freidel *et al.* [15] and Shapiro & Teixeira [22], which established the divergence structure and renormalization of the effective Barbero-Immirzi parameter, the expected order of magnitude is

$$\frac{\alpha}{M} \sim \frac{g^2}{32\pi^2}\, \frac{\gamma}{M}\, \ln\!\left(\frac{\Lambda_{\rm UV}^2}{\mu^2}\right) + \delta_{\rm NY}, \tag{8}$$

where g is the effective dimensionless axial–torsion Yukawa coupling defined by the vertex $g\,\bar{\psi}\gamma^5\gamma^a\psi\,K_a$ (with $g^2 \sim 8\pi G_N M^2\,\gamma^2/(\gamma^2+1) \sim \mathcal{O}(1)$ at the area-gap scale), $\Lambda_{\rm UV}$ is a UV scale, μ is the renormalization scale, and $\delta_{\rm NY}$ encodes the finite Nieh–Yan contribution whose precise value depends on the regularization scheme—particularly the treatment of γ_5 in dimensional regularization [22] (the 't Hooft–Veltman and Breitenlohner–Maison prescriptions yield different finite parts for parity-odd traces). We therefore **treat α/M as a phenomenological parameter constrained by data** (see Table V), with Eq. (8) providing the theoretical motivation for its existence and order of magnitude ($[(\alpha/M)\,M_{\rm Pl}] \sim 10^{-2}$), not a controlled first-principles prediction.

A one-loop RG estimate suggests logarithmic running:

$$\frac{d\alpha}{d\ln\mu} \sim -\frac{g^2}{16\pi^2} \times 2N_f, \tag{9}$$

where N_f is the number of fermion species contributing at scale μ. However, this equation inherits the same scheme dependence as the coefficient itself: its derivation requires specifying how γ_5 is handled in $d = 4-\epsilon$ dimensions and which counterterm conventions are adopted for the Nieh–Yan sector. The physical content is that α runs weakly (the loop factor $g^2/(16\pi^2) \sim 10^{-3}$ ensures perturbative suppression), so its value is approximately scale-independent over cosmological history. A first-principles derivation of α/M from non-perturbative quantum gravity (spin-foam amplitudes or lattice methods) remains an important open problem (Sec. XV).

3. Parameter Naturalness

The parent black hole mass must exceed $M_{\rm crit} = (M_{\rm Pl}^4/\rho_{\rm vac})^{1/3} \approx 10^{-3} M_\odot$, easily satisfied by any astrophysical black hole. The required dilution of inherited rotation is naturally achieved through ~ 50 e-folds of inflation.

B. Black Hole Interior and Quantum Bounce

In Loop Quantum Cosmology (LQC), holonomy corrections to the gravitational Hamiltonian constraint produce a non-singular bounce at Planck-scale densities [8]. The effective Friedmann equation is[3]

$$H^2 = \frac{8\pi G}{3}\,\rho\left[1 - \frac{\rho}{\rho_{\rm crit}}\right], \tag{10}$$

where the critical density is

$$\rho_{\rm crit} = \frac{3}{8\pi G\,\gamma^2\,\Delta} = \frac{\sqrt{3}}{32\pi^2\gamma^3}\,\rho_{\rm Pl} \simeq 0.27\,\rho_{\rm Pl}, \tag{11}$$

with $\Delta = 4\sqrt{3}\pi\gamma\,\ell_P^2$ being the LQG area gap and $\rho_{\rm Pl} \equiv c^5/(\hbar G^2)$. The numerical value $\rho_{\rm crit} \simeq 0.27\,\rho_{\rm Pl}$ corresponds to $\gamma = 0.274$ (ABCK); the DLM value $\gamma = 0.2375$ gives $\rho_{\rm crit} \simeq 0.41\,\rho_{\rm Pl}$ [8]. The range $\gamma \in [0.2375, 0.294]$ brackets both counting schemes and gives $\rho_{\rm crit} \in [0.22, 0.41]\,\rho_{\rm Pl}$. The factor $(1-\rho/\rho_{\rm crit})$ ensures that $H^2 \to 0$ as $\rho \to \rho_{\rm crit}$, producing a smooth bounce. Key properties of the bounce:

- For $\rho \ll \rho_{\rm crit}$: standard GR is recovered exactly.
- For $\rho \to \rho_{\rm crit}$: $H \to 0$ (the universe momentarily stops expanding/contracting).
- For ρ slightly below $\rho_{\rm crit}$ (contracting phase): $\dot{H} > 0$, triggering the bounce.
- The bounce creates a new expanding region with initial conditions completely determined by the parent black hole properties, with no free parameters.

In a rotating black hole, the collapsing matter carries angular momentum through the bounce. The baby universe inherits this rotation, establishing a preferred cosmic axis $\hat{\omega}^a$. This is the physical origin of cosmic parity violation in our framework.

C. Cosmic Rotation and Dark Energy

The effective cosmological constant in our framework is parameterized as:

$$\boxed{\Lambda_{\rm eff} = \Xi\,M_{\rm Pl}^2 + c_\omega\omega^2,} \quad \Xi \equiv \left[\frac{\alpha}{M}\,M_{\rm Pl}\right]\mathcal{D}_{\rm inf}, \tag{12}$$

where the first term identifies the parity-odd vacuum energy with the cosmological constant (a central *assumption*, not a derivation) and $c_\omega\omega^2$ is the vorticity contribution from the $1+3$ covariant decomposition [23]. CMB isotropy bounds give $(\omega/H)_0 < 5\times10^{-11}$ [24], so

[3] The LQC bounce (from quantum geometry holonomy corrections) is physically distinct from the Einstein-Cartan torsion bounce of Popławski [10], which produces a qualitatively similar ρ^2 repulsion through classical spin-torsion coupling at high fermion density. In this paper, we adopt the LQC effective equation for its well-studied perturbation dynamics. The ECH framework provides the broader theoretical context for the parity structure (Sec. II A 2) but is not the source of Eq. (10).

$|c_\omega|\omega^2/H_0^2 < 2.5\times10^{-21}$—rotation is completely negligible for background expansion. The dark energy scale is set entirely by $\Xi \sim 10^{-123}$ (Sec. XIV A). The expression $\rho_\Lambda = \Xi\, M_{\rm Pl}^4$ is a *parameterization* (two free parameters matching one observable), not a first-principles derivation; the "fine-tuning reduction from 10^{120} to 10^5" reparameterizes the hierarchy as sensitivity to $N_{\rm tot}$ (Sec. XIV A).

1. Inflationary Suppression

The contorsion K_{ab}, sourced by the fermion spin density, dilutes as a^{-3} during inflation. The dilution factor is:

$$\mathcal{D}_{\rm inf} = \exp[-3N_{\rm tot}] \times \left(\frac{T_{\rm reh}}{M_{\rm GUT}}\right)^{3/2}. \tag{13}$$

Matching $\rho_\Lambda \approx (2.3\ \text{meV})^4$ requires $N_{\rm tot} \approx 92$ (a fitted parameter, not predicted), reducing fine-tuning from 10^{120} to $\sim 10^5$ as sensitivity to $\Delta N_{\rm tot} \approx 4$ e-folds. This reparameterizes the fine-tuning problem as an initial-condition question ("why ∼92 e-folds?") rather than a fundamental-constant question, but does not solve the cosmological constant problem.

We *assume* $w = -1$ at late times; deriving this requires showing that the early-universe spin-torsion operator generates an IR-constant vacuum term, which has not been achieved. Four minimal routes (NJL condensate, one-loop effective action, dynamical Immirzi field, parity-sensitive CMB phenomenology) all yield negative results [25].

2. Galaxy Spin Alignment Mechanism

The galaxy spin asymmetry amplitude evolves as $A(z) = A_0(1+z)^{-p}e^{-qz}$, with $A_0 \in [0, 0.02]$. The parity-odd operator introduces systematic chirality into the tidal field, but the framework's coupling $\alpha/M \sim 10^{-21}$ GeV^{-1} underpredicts the empirical $A_0 \sim 0.003$ by > 100 orders of magnitude. The galaxy spin dipole is retained as an empirical phenomenological fit, not a prediction of the theory.

III. OBSERVATIONAL SIGNATURES AND EVIDENCE

A. CMB E-B Cross-Correlations

The parity-odd effective action generates CMB polarization signatures through cosmic birefringence: the parity-odd operator rotates the CMB polarization plane by a small angle β. For a spatially uniform (isotropic) rotation, the standard result [26] is

$$C_\ell^{EB} \approx \frac{\sin 4\beta}{2}\left(C_\ell^{EE} - C_\ell^{BB}\right) \approx 2\beta\left(C_\ell^{EE} - C_\ell^{BB}\right), \tag{14}$$

where the small-angle approximation holds for $\beta \ll 1$ rad. This produces nonzero EB power *across all multipoles*, tracking the $EE - BB$ spectrum shape—not localized to any particular ℓ range. Similarly, the induced TB cross-correlation is $C_\ell^{TB} \approx 2\beta\, C_\ell^{TE}$.

Connecting to Planck.—The Planck measurement reports $\beta \approx 0.30°$ at 2.4–2.7σ [26, 27]. Our framework's parity-odd operator (Eq. 6) is qualitatively consistent with cosmic birefringence, since it violates parity. However, deriving the photon polarization rotation angle β from our gravitational/torsion operator requires an explicit effective coupling between the parity-odd sector and the electromagnetic field—for example, a term of the standard axion-like form

$$\mathcal{L} \supset \frac{\varphi(\tau)}{4f} F_{\mu\nu}\tilde{F}^{\mu\nu}, \tag{15}$$

where φ is a pseudo-scalar field sourced by the spin-torsion sector and f is the associated decay constant, generated by integrating out torsion at one loop with an electromagnetic vertex. This coupling has not yet been derived in this work. We therefore treat the consistency between our framework's parity violation and the observed $\beta \approx 0.30°$ as suggestive, not as a quantitative prediction.

Relation between φ/f and β.—For a spatially uniform pseudo-scalar rolling over conformal time, the standard result [28] gives a uniform polarization rotation $\beta = \Delta\varphi/(2f)$, where $\Delta\varphi$ is the net field excursion between last scattering and today. This relation assumes three conditions: (i) spatial uniformity of φ over the last-scattering surface (justified if the correlation length exceeds the Hubble radius at decoupling), (ii) photon propagation along FLRW geodesics (valid for the isotropic component), and (iii) $\varphi/f \ll 1$ so that the rotation is in the small-angle regime (consistent with $\beta \approx 0.30° \approx 5\times10^{-3}$ rad). Deriving φ and f from the spin-torsion operator $(\alpha/M)\varepsilon^{abcd}K_{ab}R_{cd}$ requires computing the one-loop photon-torsion vertex and matching to the effective Lagrangian (15); this calculation is beyond the scope of the present work. We use the literature values of β as consistency benchmarks throughout.

Anisotropic component.—In addition to the uniform rotation, the cosmic rotation axis defines a preferred direction $\hat{n}$, which introduces an *anisotropic* birefringence field $\beta(\hat{n})$ with power concentrated at low multipoles. This anisotropic component contributes primarily to off-diagonal ℓ-ℓ' correlations (detectable via quadratic estimators [27]), with additional diagonal power at $\ell \lesssim 10$. A detailed derivation of the anisotropic component's spectrum from the spin-torsion mechanism is deferred to future work (Sec. XV); here we note that alternative models predict different angular spectra:

- *Axion cosmic birefringence*: Scale-invariant power in $\beta(\hat{n})$, producing EB correlations across all ℓ.
- *Chern-Simons gravity*: Peaks at $\ell \sim 100$–1000.
- *Spin-torsion (this work)*: Isotropic birefringence (all ℓ; angle not derived, requires photon-torsion coupling) plus anisotropic low-ℓ component (amplitude and shape TBD).

Observational support comes from Minami & Komatsu [26], who found cosmic birefringence in Planck data at $\beta \approx 0.35° \pm 0.14°$, inconsistent with $\beta = 0$ at 2.4σ. Subsequent analysis by Eskilt [27] found $\beta = 0.30° \pm 0.11°$ (2.7σ). A dedicated ACT DR6 analysis by Diego-Palazuelos & Komatsu [29] measured $\beta = 0.215° \pm 0.074°$ (2.9σ), providing independent confirmation from a different instrument. Joint constraints combining birefringence with early dark energy and DESI+Planck data have been explored by Yin *et al.* [30], demonstrating that nonzero β is compatible with—and potentially complementary to—solutions to the H_0 tension. A combined analysis by the SPIDER collaboration [31] using SPIDER, Planck, and ACT data yields a total polarization rotation angle (instrumental α + cosmological β) detected at $\sim 7\sigma$, though cleanly separating the instrumental and cosmological contributions remains an active challenge. The combined significance depends sensitively on the treatment of shared calibration systematics between Planck and ACT [32].

Calibration caveat.—The cosmic birefringence signal is degenerate with miscalibration of the instrumental polarization angle ψ [26]. Minami & Komatsu's method breaks this degeneracy using the galactic foreground EB signal as a self-calibration anchor, assuming vanishing intrinsic foreground EB—an assumption that has been questioned for polarized thermal dust. Independent validation from experiments with different optics and calibration strategies (Simons Observatory, LiteBIRD) is essential. The isotropic birefringence value ($\beta \approx 0.30°$) can be tested with existing and near-term data; the anisotropic low-ℓ component requires full-sky, cosmic-variance-limited polarimetry (LiteBIRD).

Detectability.—The isotropic signal has been detected at 2.4–2.7σ by Planck and 2.9σ by ACT DR6 [29], with significance expected to further improve with LiteBIRD [33] (cosmic-variance limited below $\ell \sim 10$). However, confirming the spin-torsion origin—as opposed to other birefringence sources—requires measuring the anisotropic component's angular spectrum and cross-correlating the birefringence axis with the galaxy spin dipole axis, both of which are accessible to the next generation of experiments.

B. Galaxy Spin Asymmetry: A Contested Anomaly

Several groups have reported a dipole asymmetry in galaxy spin handedness ($A_0 \sim 0.003$, axis near the CMB kinematic dipole) [34–36], but independent reanalyses [37, 38] find results consistent with isotropy. The minimal ECH framework underpredicts A_0 by > 100 orders of magnitude (Sec. II C 2); the galaxy spin dipole is therefore an empirical phenomenological fit, not a framework prediction. Our framework survives a definitive null result: CMB parity violation (2.4–2.9σ from Planck and ACT DR6 [26, 27, 29]) provides independent evidence entirely decoupled from galaxy morphology.

TABLE II. Independent verification results from frozen MCMC chains (Cobaya v3.6.1, CAMB v1.6.5). All values are posterior means $\pm 1\sigma$. The full-tension dataset includes SH0ES H_0 and DES S_8 priors; Planck+BAO+SN does not.

Parameter	Full-tension	Planck+BAO+SN
H_0 [km/s/Mpc]	67.68 ± 1.06	67.79 ± 1.09
$\Delta N_{\rm eff}$	-0.020 ± 0.169	$+0.065 \pm 0.17$
σ_8	0.803 ± 0.008	0.812 ± 0.009
S_8	0.814 ± 0.008	0.831 ± 0.018
Ω_m	0.308 ± 0.005	0.312 ± 0.006
τ	0.054 ± 0.007	0.056 ± 0.007
n_s	0.965 ± 0.006	0.967 ± 0.006
Chains	6	6
Total samples	176,840	132,949
Worst $\hat{R} - 1$	0.001	0.003
Min ESS	4,744	4,692

C. Cosmological Tensions: H_0 and σ_8

The bounce scenario motivates extending ΛCDM by $\Delta N_{\rm eff}$ (particle production at the bounce) and $(\omega/H)_0$ (angular momentum transfer), treated as phenomenological parameters. Ω_k is fixed to zero (mandated by 92 e-folds of inflation). The *original* MCMC analysis (which included the SH0ES H_0 prior) yielded $H_0 = 69.2 \pm 0.8$, $\sigma_8 = 0.785 \pm 0.016$; however, independent verification (Sec. III D) shows these were driven by the SH0ES prior, not by the $\Delta N_{\rm eff}$ extension. The spin-torsion framework alone does not resolve cosmological tensions.

D. Independent Verification Results

Independent verification using Cobaya v3.6.1 with Planck NPIPE CamSpec TTTEEE + lowl TT/EE + lensing has produced two frozen dataset combinations with publication-quality convergence, plus an ongoing Planck-only run (114,992 raw samples, 436,799 weighted) that also finds $\Delta N_{\rm eff}$ consistent with zero. Total MCMC program: 424,181 raw samples across 3 dataset combinations.

Key finding.—Both frozen datasets find $\Delta N_{\rm eff}$ consistent with zero (-0.020 and $+0.065$, both within 1σ of $\Delta N_{\rm eff} = 0$) and H_0 consistent with Planck ΛCDM at 0.3σ, confirming that the $\Delta N_{\rm eff}$ extension alone does not resolve the Hubble tension. Current data neither require

nor exclude a small positive $\Delta N_{\rm eff}$ from the spin-torsion sector; CMB-S4 ($\sigma(N_{\rm eff}) \sim 0.03$) will provide the first precision test.

Independent cross-validation.—Liu *et al.* [39] constrained an EC torsion model using DESI DR2 + PantheonPlus + DES Y5 + Planck 2018, finding torsion preferred by AIC (ΔAIC $= -5.7$ to -6.6). Our MCMC agrees at 0.5σ in H_0 and 0.4σ in σ_8, providing independent cross-validation.

IV. ENHANCED THEORETICAL DERIVATIONS

The one-loop motivation for the parity-odd coefficient, the vacuum energy from fermion condensates, and the derivation of cosmological parameters from $\Lambda_{\rm eff}$ are documented in the supplementary material. In summary: α/M is treated as a phenomenological parameter (Sec. II A 2), the condensate mechanism yields a vacuum energy $\sim 10^{44}$ times too large (not a viable DE source), and the MCMC-fit parameters are derived in Sec. VII.

V. DATA METHODS: GALAXY SPIN ANALYSIS

Galaxy spin dipole analysis uses published CW/CCW labels from Shamir [35, 40] fit with a hierarchical Bayesian model (Appendix A). The minimal ECH framework underpredicts the observed amplitude $A_0 \sim 0.003$ by > 100 orders of magnitude; the signal is included as a contested anomaly, not a framework prediction. See the supplementary material for full methodology.

VI. DATA METHODS: CMB E-B ANALYSIS

Birefringence measurements are adopted from the published literature: $\beta = 0.30^\circ \pm 0.11^\circ$ (Planck NPIPE [27]) and $\beta = 0.215^\circ \pm 0.074^\circ$ (ACT DR6 [29]). No independent map-level CMB analysis is performed. The spectator ALP analysis (Sec. XIV C) uses these published values.

VII. COSMOLOGICAL FITS AND MODEL COMPARISON

A. Datasets and Configuration

We analyze four dataset combinations: (1) Planck 2018 NPIPE [1]; (2) +DESI 2024 DR1 BAO [6]; (3) +Pantheon+; (4) +SH0ES H_0 prior [3] + DES Y3 S_8 [5]. Parameter estimation uses Cobaya [41] (v3.5 original; v3.6.1 verification) with stock CAMB and $\Delta N_{\rm eff}$ as a free parameter—no custom CAMB modifications. The extended parameter space adds $\{\Delta N_{\rm eff}, (\omega/H)_0\}$ to ΛCDM, with Ω_k fixed to zero (mandated by 92 e-folds). Reproducibility materials are at https://github.com/Hubify-Projects/bigbounce/tree/v2.1.0/reproducibility.

B. Results

The Bayesian evidence is dataset-dependent:

$$\ln \mathcal{Z}_{\rm ST} - \ln \mathcal{Z}_{\Lambda\rm CDM} = \begin{cases} -1.2 \pm 0.3 & \text{Planck+BAO} \\ +4.8 \pm 0.5 & \text{Full tension} \end{cases} \tag{16}$$

With Planck+BAO alone, the Occam penalty slightly disfavors the model; the preference emerges when tension data are included. The fine-tuning comparison (10^5 vs. 10^{120} for ΛCDM) is a reparameterization as sensitivity to $N_{\rm tot}$, not a resolution (Sec. XIV A). The decisive test is detection of correlated parity-odd signatures (CMB E-B, galaxy spin dipole axis), not tension resolution alone.

VIII. SYSTEMATIC ANALYSIS

Combined detection significance is estimated using inverse-variance weighting of the CMB birefringence measurements (Sec. XIV C). Null tests for the galaxy spin and CMB channels follow the standard protocols described in the original analyses [26, 35]. For the $f_{\rm NL}$ channel, systematic uncertainties including GR projection effects, b_ϕ bias, and photo-z degradation are analyzed in the companion paper [42]. The primary residual systematic for the MCMC verification is the dataset-dependent $\Delta N_{\rm eff}$: the full-tension dataset (including SH0ES) pulls H_0 upward, while the Planck+BAO+SN dataset recovers standard values (Sec. III D).

IX. FALSIFICATION CRITERIA

The framework's surviving predictions are testable: (1) LiteBIRD ($\sigma(\beta) \approx 0.03^\circ$, early 2030s) will confirm or exclude the ALP birefringence at $\sim 9\sigma$; (2) SPHEREx (first science data $\sim$2028) will test $f_{\rm NL} = -35/8$ at 4–6σ via the galaxy bispectrum; (3) MCMC parameter values (H_0, σ_8, $\Delta N_{\rm eff}$) are already consistent with standard ΛCDM (no tension resolution claimed). The framework has already self-falsified several earlier claims through its own MCMC verification (Sec. III D).

X. RELATED WORK

This work builds on rotating cosmologies (Gödel 1949), Einstein-Cartan theory (Hehl *et al.* [9]), Popławski's torsion bounce and black hole universe scenario [10–12], the

TABLE III. Bayesian model comparison (full tension dataset). Bayes factors estimated via Savage-Dickey density ratio.

Model	k	$\chi^2_{\rm eff}$	AIC	BIC	$\ln B$
ΛCDM	6	1156.2	1168.2	1195.5	0.0
wCDM	7	1154.8	1168.8	1199.2	-0.5
Spin-Torsion	**7**	**1148.3**	**1162.3**	**1194.8**	**+4.8**

Holst/Nieh-Yan parity structure (Freidel *et al.* [15], Mercuri [16, 17]), and cosmic birefringence detections (Minami & Komatsu [26]). Recent independent support includes Liu *et al.* [14] (EC torsion preferred by AIC), Legner *et al.* [43] (torsion condensation), and Alam *et al.* [44] (non-singular bounces in modified gravity). No prior work assembles these into a single quantitative framework with systematic barrier testing.

XI. STRUCTURAL BARRIERS TO FIRST-PRINCIPLES DARK ENERGY

We tested 7 foundation mechanism classes (Foundations A–G) and 7 additional observational channels (Branches H–O, plus the ECH perturbation gates) for the possibility of connecting the bounce to late-time dark energy or producing distinctive observable signatures. Each test yielded a named structural barrier.

A. Barrier 1: Mass-Coupling Lock (Foundation A)

In Poincaré gauge theory (PGT), the most general torsion Lagrangian includes propagating spin-2 and spin-0 torsion modes with masses m_T set by the PGT coupling constants $\{t_i\}$. For these modes to act as dark energy, they would need to be ultralight ($m_T \sim H_0 \sim 10^{-33}$ eV) and couple to matter at cosmologically relevant strength.

The mass-coupling lock arises because the effective coupling is:

$$g_{\rm eff} \sim \frac{1}{M_{\rm Pl}\sqrt{|t_3|}} \tag{17}$$

where t_3 is the PGT coupling. For ultralight masses ($|t_3| \sim M_{\rm Pl}^2/H_0^2$), the coupling becomes $g_{\rm eff} \sim H_0/M_{\rm Pl}^2 \sim 10^{-61}$—far too weak for any observable effect. To achieve $g_{\rm eff} \sim 1$, one needs $|t_3| \sim 1/M_{\rm Pl}^2$, giving $m_T \sim M_{\rm Pl}$ (Planck-mass torsion, not dark energy).

The fine-tuning required to simultaneously achieve $m_T \sim H_0$ and $g_{\rm eff} \sim \mathcal{O}(1)$ is:

$$\frac{m_T^2}{m_T^2|_{\rm natural}} \sim \frac{H_0^2}{M_{\rm Pl}^2} \sim 10^{-122} \tag{18}$$

equivalent to the standard cosmological constant fine-tuning problem. The barrier transfers rather than solves the fine-tuning.

Graviton loop corrections generate $\delta m_T^2 \sim M_{\rm Pl}^2/(16\pi^2)$, requiring cancellation at the level of 1 in 10^{57}.

B. Barrier 2: Topological-Shift Duality (Foundation B)

Foundation B investigated whether the Nieh-Yan topological term could break the mass-coupling lock by providing a non-topological mass term in metric-affine gravity (MAG). In MAG, the Nieh-Yan term $\int T^a \wedge T_a - e^a \wedge e^b \wedge R_{ab}$ is indeed non-topological (unlike in standard EC theory).

However, a duality emerges: configurations that protect the pseudoscalar mass (through the topological structure) necessarily eliminate the geometric content (the field becomes a standard ALP after torsion elimination). Conversely, configurations that preserve geometric content cannot protect the mass. This *topological-shift duality* means:

$$\text{Mass protection} \iff \text{No geometric fingerprint} \tag{19}$$

After exact torsion elimination (to all orders in ϕ/f_ϕ), the effective action reduces to standard ALP electrodynamics with no operators beyond those already present in generic scalar-tensor theory.

C. Barrier 3: Scalar-Tensor Universality (Foundation C)

For scalar field matter on FRW backgrounds, the background torsion and non-metricity vanish identically:

$$T_0 = Q_0 = 0 \quad \text{(exact on FRW with scalar matter)} \tag{20}$$

This is because FRW symmetry (homogeneity + isotropy) admits no preferred spatial direction for torsion or non-metricity to point in when the matter is a scalar field. Environmental mass mechanisms (chameleon-like effects from torsion) therefore reduce exactly to standard scalar-tensor theory on cosmological backgrounds, with no distinctive geometric fingerprint.

D. Barrier 4: Planck Suppression (Foundation D)

Disformal couplings (terms involving $\partial_\mu\phi\,\partial_\nu\phi$ in the effective metric) could in principle produce distinctive signatures. However, in the connection-coupling framework of ECH, each interaction vertex carries only one $\partial\phi$ factor (from the single derivative in the torsion-scalar

#	Barrier	Source	Mechanism Blocked
1	Mass-Coupling Lock	Found. A	Propagating torsion as DE
2	Topological-Shift Duality	Found. B	Geometric pseudoscalar mass protection
3	Scalar-Tensor Universality	Found. C	Distinctive geometric content on FRW
4	Planck Suppression	Found. D	Disformal / connection coupling effects
5	Scale Separation	Found. E	Global vacuum integral coupling
6	Attractor-Sensitivity Dilemma	Found. F	Initial-condition transfer to DE
7	Parameter Immunity	Found. G	Cyclic vacuum selection
8	Parity-Even Interaction	Branch H	Tensor chirality from the bounce
9	Liouville Conservation	Branch J	Reversible state selection
10	UV→IR Specificity Dilemma	Branch L	Generic vs. bounce-specific bridge
11	Decoupling Universality	Branch L/M	Light gauge field coupling
12	Vacuum Amplification Ceiling	Branch M	Gravitational wave amplitude
13	Gravitational Democracy	Branch N/O	Relics, baryogenesis, vacuum transitions
14	Perturbation Transparency	ECH Gates	ECH-specific perturbation signatures

TABLE IV. The 14 structural barriers. Each closes a distinct mechanism class for connecting the bounce to late-time observables.

coupling), while disformal effects require two. The resulting operators are suppressed by:

$$\frac{\text{Disformal effect}}{\text{Conformal effect}} \sim \frac{k^2}{M_{\rm Pl}^2} \sim 10^{-122} \tag{21}$$

at cosmological scales, rendering all distinctive geometric effects unobservable.

E. Barrier 5: Scale Separation (Foundation E)

Global vacuum integrals (attempts to connect the bounce vacuum energy to the late-time cosmological constant through spacetime-volume-averaged quantities) fail due to extreme scale separation:

$$\frac{V_4^{\rm bounce}}{V_4^{\rm total}} \sim \frac{t_{\rm bounce}^4}{t_0^4} \sim \frac{t_{\rm Pl}^4}{(10^{17}\,{\rm s})^4} \sim 10^{-244} \tag{22}$$

The bounce occupies a vanishingly small fraction of the total spacetime volume. No averaging procedure can amplify the bounce-scale vacuum energy to affect late-time dynamics.

F. Barrier 6: Attractor-Sensitivity Dilemma (Foundation F)

Attempts to transfer bounce initial conditions to late-time dark energy face a dilemma:

- If the late-time dynamics has an *attractor*, the system forgets its initial conditions—including any information from the bounce.
- If the dynamics is *sensitive* to initial conditions, it requires fine-tuning of those conditions to produce the observed dark energy—reintroducing the problem.

There is no middle ground: either the bounce information is washed out (attractor) or it requires tuning (sensitivity).

G. Barrier 7: Parameter Immunity (Foundation G)

In cyclic/ekpyrotic models, the vacuum energy at late times is set by the continuous parameter μ^4 in the potential, which is *immune* to the bounce dynamics:

$$\Lambda_{\rm eff} = \mu^4 + \mathcal{O}(e^{-M_{\rm Pl}/\sigma}) \approx \mu^4 \tag{23}$$

The bounce introduces corrections that are exponentially suppressed by the Planck mass. The vacuum energy is a free parameter, not a prediction.

H. Barrier 8: Parity-Even Interaction (Branch H)

The spin-torsion effective interaction obtained after integrating out torsion is:

$$\mathcal{L}_{\rm eff} \supset \frac{3}{16}\frac{(J_\mu^5)^2}{M_{\rm Pl}^2} \tag{24}$$

where $J_\mu^5 = \bar\psi\gamma^\mu\gamma^5\psi$ is the axial fermion current. Despite the presence of γ^5, the interaction $(J^5)^2$ is *parity-even* (a pseudovector squared is a scalar). This means:

- No tensor chirality: $\Delta v \equiv v_R - v_L = 0$ exactly
- No gravitational-wave birefringence
- No TB/EB CMB parity violation from the bounce

FRW isotropy further kills all spatial parity-odd backgrounds.

I. Barrier 9: Liouville Conservation (Branch J)

Attempts to use the bounce as a "state selector"—choosing a preferred vacuum or field configuration from a broader landscape—are blocked by Liouville's theorem. In Hamiltonian mechanics, phase-space volume is conserved under unitary evolution:

$$\frac{d}{dt}\int_\Gamma d^n q\, d^n p = 0 \tag{25}$$

where Γ is any region of phase space. The bounce, being governed by the modified Friedmann equation (Eq. 10), is a smooth, time-reversible Hamiltonian flow. It cannot irreversibly contract the accessible phase-space volume.

The consequence for dark energy is direct: if the pre-bounce phase space contains a measure-zero set of trajectories leading to the observed $\Lambda_{\rm eff}$, the post-bounce phase space contains the same measure-zero set. The bounce cannot amplify the probability of landing on a trajectory with $\rho_\Lambda \approx (2.3\ \text{meV})^4$. Any mechanism that appears to select a preferred vacuum through the bounce must, upon closer inspection, either (a) have the selection already encoded in the initial conditions (shifting the fine-tuning to the contracting phase) or (b) invoke dissipative/decoherence effects that violate unitarity.

Entropy production during the bounce (e.g., particle creation at near-Planck densities) does break time-reversal symmetry, but the resulting entropy increase is generic—it does not preferentially select cosmological-constant-scale vacuum energies over any other scale. The entropy is $\Delta S \sim \rho_{\rm crit}/T_{\rm bounce} \sim \mathcal{O}(M_{\rm Pl}^3)$, which is Planck-scale information, not IR-scale vacuum selection.

J. Barrier 10: UV→IR Specificity Dilemma (Branch L)

Any mechanism bridging bounce-scale (UV) physics to cosmological-scale (IR) dark energy must make a choice: be *generic* (arising from general principles applicable to any UV completion) or be *specific* (deriving from detailed ECH/LQC structure). Both choices fail:

Generic bridges produce effects indistinguishable from standard scalar-tensor theory. If the bridge depends only on the existence of a bounce at some critical density ρ_c and a subsequent expansion, its IR predictions are captured by an effective field theory with operators organized by the hierarchy:

$$\mathcal{L}_{\rm eff} = M_{\rm Pl}^2 R + c_1 \frac{R^2}{M_{\rm Pl}^2} + c_2 \frac{(\nabla\phi)^4}{M_{\rm Pl}^4} + \cdots \tag{26}$$

where the Wilson coefficients c_i are $\mathcal{O}(1)$ numbers set at the UV scale. These operators produce late-time effects suppressed by $H_0^2/M_{\rm Pl}^2 \sim 10^{-122}$. No generic bridge can overcome this hierarchy without invoking a light scalar with mass $m \sim H_0$—which is precisely the cosmological constant problem in a different guise.

Specific bridges require detailed knowledge of the bounce dynamics at Planck density to set IR parameters. But any IR parameter that depends sensitively on Planck-scale details is subject to radiative corrections of order $\delta m^2 \sim M_{\rm Pl}^2/(16\pi^2)$, requiring cancellation at 1 part in 10^{57} (the same hierarchy as Barrier 1). The specificity that makes the mechanism distinctive also makes it radiatively unstable.

This dilemma is a manifestation of the technical naturalness problem [45]: a small parameter $(H_0/M_{\rm Pl})$ is natural only if setting it to zero enhances the symmetry of the theory. No bounce mechanism provides such a symmetry.

K. Barrier 11: Decoupling Universality (Branches L/M)

Light gauge fields (photons, gravitons at cosmological wavelengths) decouple from Planck-scale torsion modes with universal efficiency, governed by the Appelquist-Carazzone decoupling theorem. For a heavy torsion mode of mass $m_T \sim M_{\rm Pl}$, its contribution to the vacuum polarization of a massless gauge field at momentum $k \ll m_T$ is:

$$\Pi(k^2) \sim \frac{g_{\rm eff}^2}{16\pi^2}\left[\frac{k^2}{m_T^2} + \mathcal{O}\left(\frac{k^4}{m_T^4}\right)\right] \tag{27}$$

where $g_{\rm eff}$ is the torsion-gauge coupling. At cosmological scales ($k \sim H_0$):

$$\frac{\Pi(H_0^2)}{\Pi(M_{\rm Pl}^2)} \sim \frac{H_0^2}{M_{\rm Pl}^2} \sim 10^{-122} \tag{28}$$

This suppression is not specific to ECH or any particular torsion theory—it follows from general principles of effective field theory. The bounce imprints its physics at scale $M_{\rm Pl}$; by the time this information propagates to scale H_0 through gauge-sector loops, it is suppressed by 122 orders of magnitude.

The only escape from decoupling universality is a torsion mode that is itself ultralight ($m_T \sim H_0$), but this returns to the mass-coupling lock of Barrier 1: achieving $m_T \sim H_0$ requires fine-tuning at the level of 10^{-122}. The combination of Barriers 1 and 11 forms a closed loop: heavy torsion modes decouple from IR physics, and light torsion modes require the same fine-tuning they were meant to explain.

L. Barrier 12: Vacuum Amplification Ceiling (Branch M)

The gravitational wave energy density from a PGT-type bounce is bounded by:

$$\Omega_{\rm GW}(f) \propto \left(\frac{H_{\rm bounce}}{M_{\rm Pl}}\right)^2 \propto \left(\frac{f_{\rm bounce}}{f_{\rm Pl}}\right)^4 \tag{29}$$

For any sub-Planckian bounce, $\Omega_{\rm GW}$ is catastrophically small. The characteristic frequency is $f_{\rm bounce} \sim 10^9$–10^{10} Hz (GHz), with zero overlap with any planned detector (LIGO at 10–10^3 Hz, LISA at 10^{-4}–10^{-1} Hz). The detector gap is at least 10^{17} in amplitude.

M. Barrier 13: Gravitational Democracy (Branches N/O)

Torsion-mediated baryogenesis or relic production fails because torsion couples democratically to all fermion species ($\sim 1\%$ torsion contribution per species), with no mechanism to preferentially produce baryons over antibaryons or specific dark matter candidates. Vacuum transitions at the bounce are blocked by the bounce-vacuum decoupling: the bounce is too brief and too symmetric to trigger irreversible phase transitions.

N. Barrier 14: Perturbation Transparency

See Section XII for the full proof. In summary: for canonical scalar field matter, torsion vanishes identically at all perturbation orders, rendering the Holst term topological and the Barbero-Immirzi parameter invisible.

XII. THE PERTURBATION-TRANSPARENCY THEOREM

A. Statement

In minimal Einstein-Cartan-Holst gravity with canonical scalar field matter, the Holst term is dynamically inert for both scalar and tensor perturbations at all orders. The Barbero-Immirzi parameter γ is invisible in all perturbation observables.

B. Proof (Scalar Sector)

The argument proceeds in five steps:

1. **Zero spin density.** A canonical scalar field ϕ has spin density $S^\lambda{}_{\mu\nu} = 0$ (by definition of "canonical"—no spinor indices, no intrinsic angular momentum).

2. **Zero torsion.** In Einstein-Cartan theory, the torsion tensor is algebraically determined by the spin density: $T^\lambda{}_{\mu\nu} = 8\pi G\,(S^\lambda{}_{\mu\nu} + \delta^\lambda_{[\mu} S_{\nu]} + \ldots)$. With $S = 0$, we have $T^\lambda{}_{\mu\nu} = 0$ at all perturbation orders.

3. **Connection reduces to Levi-Civita.** With $T = 0$, the full connection $\Gamma^\lambda{}_{\mu\nu} = \mathring{\Gamma}^\lambda{}_{\mu\nu}$ (Christoffel symbols only).

4. **Holst term becomes topological.** The Holst term $\frac{1}{2\gamma}\int \epsilon^{IJ}{}_{KL}\, e^K \wedge e^L \wedge F_{IJ}$ evaluated with the Levi-Civita connection evaluates to $\frac{1}{2}\epsilon^{\mu\nu\rho\sigma} R_{\mu\nu\rho\sigma}(\mathring{\Gamma})$, which vanishes identically for a torsion-free Riemann tensor by the first Bianchi identity $R_{[\mu\nu\rho]\sigma} = 0$ (verified numerically: $|\varepsilon^{\mu\nu\rho\sigma} R_{\mu\nu\rho\sigma}| < 10^{-15}$ across 1,000 random Riemann tensors satisfying the Bianchi symmetry).

5. **No equations of motion.** A total derivative contributes zero to the variational equations at all orders in perturbation theory.

C. Extension to Tensor Sector

The same five-step argument applies to tensor perturbations. With $T = 0$, the gravitational action reduces to the Einstein-Hilbert form plus a topological term. The tensor perturbation equation is:

$$h''_{ij} + 2\mathcal{H} h'_{ij} + k^2 h_{ij} = 0 \tag{30}$$

with no parity-dependent modifications. The left and right circular polarization modes propagate identically:

$$v_R(k,\eta) = v_L(k,\eta) \quad \Rightarrow \quad \Delta v \equiv v_R - v_L = 0 \quad \text{(exact)} \tag{31}$$

This means: no gravitational-wave birefringence, no tensor chirality, and no TB/EB CMB parity violation from the ECH mechanism. This result was independently confirmed by the Branch H parity-tensor analysis (Barrier 8), which proved that the spin-torsion effective interaction $(J^5)^2$ is parity-even.

D. Explicit Verification: The Holst Term in Perturbation Theory

To make the argument fully explicit, consider the ECH action:

$$S_{\rm ECH} = \frac{M_{\rm Pl}^2}{2}\int d^4x\,\sqrt{-g}\left[R(\Gamma) + \frac{1}{\gamma}\widetilde{R}(\Gamma)\right] + S_{\rm matter}[\phi, g] \tag{32}$$

where $\widetilde{R} = \frac{1}{2}\epsilon^{\mu\nu\rho\sigma} R_{\mu\nu\rho\sigma}$ is the dual Riemann contraction, and Γ is the full (torsionful) connection.

Expanding the metric to second order ($g_{\mu\nu} = \bar{g}_{\mu\nu} + \delta g^{(1)}_{\mu\nu} + \delta g^{(2)}_{\mu\nu} + \ldots$) and the scalar field ($\phi = \bar{\phi} + \delta\phi^{(1)} + \delta\phi^{(2)} + \ldots$):

At *each perturbation order*, the torsion equation of motion gives $T = 0$ (because $S_{\rm matter}$ for a canonical scalar has zero spin density at every order). Therefore $\Gamma = \mathring{\Gamma}$ at every order, and the Holst dual evaluates to:

$$\widetilde{R}(\mathring{\Gamma}) = \frac{1}{2}\epsilon^{\mu\nu\rho\sigma} R_{\mu\nu\rho\sigma}(\mathring{\Gamma}) = 0 \quad \text{(by the first Bianchi identity)} \tag{33}$$

This holds at zeroth, first, second, and third order in perturbation theory. In particular, the *cubic action* for ζ (the Maldacena action that determines the bispectrum) receives *zero* contribution from the Holst term. The bispectrum is therefore identical to the standard GR result.

E. What Would Break the Transparency

The transparency theorem fails if *any* of the following conditions hold:

1. **Fermionic matter:** If the matter sector includes fermions (spinors), the spin density $S^{\lambda}{}_{\mu\nu} \neq 0$ and torsion is sourced. The Holst term then contributes dynamically. However, fermionic contributions to torsion are Planck-suppressed at cosmological densities and negligible during the matter-contraction phase relevant for the bispectrum. Note that the EC torsion bounce of Popławski [10] *requires* fermionic spin density and therefore falls outside the scope of this theorem. Our perturbation analysis adopts the LQC bounce (Sec. II B), which operates with scalar field matter where the theorem applies.

2. **Propagating torsion (Poincaré gauge theory):** If the gravitational action includes kinetic terms for torsion ($\sim T_{\mu\nu\rho}T^{\mu\nu\rho}$), torsion becomes dynamical rather than algebraic. The Holst term then generates non-trivial dynamics. However, this is *not* Einstein-Cartan theory—it is a different theory entirely (PGT), and our Foundation A analysis showed it faces the mass-coupling lock (Barrier 1).

3. **Non-minimal scalar-torsion coupling:** Terms like $\phi^2 T^2$ or $\phi\nabla_\mu T^\mu$ could source torsion from the scalar field. However, these are ad hoc additions to the minimal ECH action, and our Foundation C analysis showed they reduce to standard scalar-tensor theory on FRW backgrounds (Barrier 3).

4. **Higher-derivative corrections:** Terms like ∇T or R^2 in the gravitational action could make torsion propagate. These are UV corrections expected at the Planck scale and are negligible during the matter-contraction phase ($\rho \ll M_{\rm Pl}^4$).

In summary: the transparency is robust within the minimal ECH framework. Breaking it requires going beyond minimal ECH, and all such extensions have been tested and closed by Barriers 1–4.

F. Implications

The perturbation-transparency theorem applies to the ECH parity structure (Holst term, four-fermion interaction, parity-odd operator), establishing that these have no effect on perturbation observables for canonical scalar field matter. The bounce itself is realized by the LQC effective equation (Sec. II B), which operates on scalar field matter where ECH is indeed transparent. During the matter-contraction phase relevant for the bispectrum, the matter content is a scalar field and the ECH sector is inert.

This result has a positive interpretation: the observable predictions of a matter bounce (principally $f_{\rm NL} = -35/8$) depend only on the contracting-phase dynamics, which are governed by scalar field matter where ECH is transparent. The bispectrum does not depend on the UV completion that produces the bounce—whether LQC holonomy corrections, ECH torsion with fermions, or another mechanism—making the prediction *mechanism-independent* and thus more robust.

XIII. THE HYBRID DARK-ENERGY LOOPHOLE

We considered the phenomenological route of appending late-time dynamical-dark-energy freedom (e.g., CPL w_0w_a parametrization) to the bounce model. This was explored across 7 disguised forms:

1. Direct w_0w_a addition to the background
2. Quintessence scalar with bounce-motivated initial conditions
3. Curvaton-derived late-time potential
4. Vacuum energy from cyclic boundary conditions
5. Torsion-induced effective $w(z)$
6. Holst-term residual as effective DE
7. ALP rolling as late-time acceleration

All 7 forms were rejected on the following grounds: adding w_0w_a to a bounce model produces the same fit improvement as adding w_0w_a to ΛCDM, with no additional theoretical content from the bounce. None of the 309,789 MCMC posterior samples in this program used w_0 or w_a as free parameters. The loophole was explored theoretically but never implemented computationally, because its implementation would not constitute first-principles evidence for bounce cosmology.

XIV. DISCUSSION

A. The Inflationary Suppression Factor

The constant contribution to $\Lambda_{\rm eff}$ is modeled as emerging from the interplay between a parity-odd spin-torsion

interaction and inflationary dilution. We define the *inflationary suppression factor*:

$$\Xi \equiv \left[\frac{\alpha}{M} M_{\rm Pl}\right] \times \mathcal{D}_{\rm inf}, \tag{34}$$

a dimensionless quantity encoding the net suppression of the Planck-scale parity-odd coefficient. The vacuum energy density is then $\rho_\Lambda = \Xi M_{\rm Pl}^4$, so the observed $\rho_\Lambda \approx (2.3\ \text{meV})^4$ corresponds to $\Xi \approx 10^{-123}$—the familiar cosmological constant hierarchy, here decomposed as $\Xi = 10^{-2} \times \mathcal{D}_{\rm inf}$ with $\mathcal{D}_{\rm inf} \sim 10^{-121}$ (Sec. II C 1).

The physical interpretation is straightforward: $[(\alpha/M)\, M_{\rm Pl}] \sim 10^{-2}$ measures the dimensionless strength of parity violation in quantum gravity at one loop, while $\mathcal{D}_{\rm inf}$ captures how much inflation dilutes this primordial effect. Their product—a single bridge between Planck-scale microphysics and cosmic acceleration—translates the "why is Λ so small?" question into "why did inflation last $\sim$92 e-folds?"—a question with concrete dynamical answers in the bounce-to-inflation transition. The factor Ξ provides a testable connection between UV quantum gravity and IR cosmological acceleration through the falsification criteria defined in Sec. IX.

B. Theoretical Implications

Detection of the parity-odd signatures would constrain LQG parameters (γ, ρ_c) from cosmological data, establish an empirical UV-IR connection mediated by inflationary dilution, and provide evidence for parity violation in quantum gravity. A detailed discussion of implications for black hole interior physics and the origin of dark energy is given in the supplementary material.

C. Cosmic Birefringence: Spectator ALP Consistency Check

Note: This subsection presents a secondary consistency check using a spectator ALP model. The ALP is independent of bounce cosmology and not derived from minimal ECH (which does not produce the required photon-torsion coupling). The model class was previously studied by Fujita et al. [18]; our contribution is the ECH-motivated parameter identification and independent inference. This material is included for completeness and does not affect the paper's central results (the barrier catalog and perturbation-transparency theorem).

Cosmic birefringence—a uniform rotation of CMB linear polarization—has been reported at 2.5–2.9σ by independent analyses of Planck [26, 27] and ACT DR6 [29] data. The parity-odd structure of the Holst action provides heuristic motivation for a spectator ALP with $f_a \sim M_{\rm Pl}$ and $m \sim H_0$.

ALP field evolution.—Numerical integration of the ALP equation of motion $\ddot{\phi} + 3H\dot{\phi} + m^2 f_a \sin(\phi/f_a) = 0$ in a ΛCDM background (Planck 2018 parameters) yields the field displacement from recombination to today:

$$\Delta\phi/f_a \approx 0.65 \quad (m = H_0,\ \theta_i = 1), \tag{35}$$

where $\theta_i = \phi_{\rm ini}/f_a$ is the initial misalignment angle. The displacement is $\mathcal{O}(1)$, as the field rolls during the Λ-dominated transition era ($z \lesssim 1$). Across the natural parameter range $m/H_0 \in [1, 3]$, $\theta_i \in [0.5, 2]$, the displacement varies over $\Delta\phi/f_a \in [0.2, 1.1]$.

Birefringence prediction.—The rotation angle is $\beta = (\alpha_{\rm EM}\, C_{a\gamma})/(4\pi f_a) \times \Delta\phi$, where $C_{a\gamma}$ is the integer anomaly coefficient. For natural parameters ($C_{a\gamma} = 8$, $\theta_i = 1$, $m \approx 2\, H_0$):

$$\beta \approx \frac{\alpha_{\rm EM} \times 8}{4\pi} \times 1.07 \approx 0.29^\circ, \tag{36}$$

consistent with the observed signal. The prediction spans $\beta \approx 0.17$–0.43° over $C_{a\gamma} \in [4, 12]$, $m/H_0 \in [1, 3]$, $\theta_i \in [0.5, 2]$, comfortably bracketing the observed value without fine-tuning. This ALP model class was previously studied by Fujita *et al.* [18]; our analysis confirms their results and adds the ECH motivation and numerical MCMC constraints described below.

Summary-likelihood combination.—Combining $\beta = 0.30^\circ \pm 0.11^\circ$ (Planck NPIPE [27]) and $\beta = 0.215^\circ \pm 0.074^\circ$ (ACT DR6 [29]) via inverse-variance weighting:

$$\beta_{\rm combined} = 0.242^\circ \pm 0.061^\circ \quad (3.9\sigma \text{ from zero}). \tag{37}$$

A Savage-Dickey density ratio gives BF($\beta \neq 0$) ≈ 176 (prior-dependent; the value shifts with the assumed β range).

MCMC parameter estimation.—Dedicated MCMC sampling of the ALP parameter space (3 configurations, 9,720 total accepted samples) yields: $\beta_{\rm ALP} = 0.336^\circ \pm 0.107^\circ$ (ALP model, $C_{a\gamma} = 8$ fixed), consistent with the model-independent fit $\beta_{\rm free} = 0.344^\circ \pm 0.096^\circ$ and the observed $\beta_{\rm obs} = 0.342^\circ \pm 0.094^\circ$ (Eskilt *et al.*joint analysis). All three are within 1σ, confirming internal consistency. The coupling-misalignment product is $C_{a\gamma} \times \theta_i = 3.4 \pm 1.1$. Priors: $\theta_i \in [0.01, \pi]$ flat, $\log_{10}(m/\text{eV}) \in [-35, -30]$ flat, $C_{a\gamma} \in [1, 30]$ flat. These sample sizes (720–6,840) are modest; the posteriors are converged ($\hat{R} - 1 < 0.01$) but tail estimates are limited.

LiteBIRD forecast.—LiteBIRD is projected to achieve $\sigma(\beta) \approx 0.03^\circ$, contingent on the self-calibration strategy and systematic error budget [33]. For $\beta = 0.27^\circ$, this gives $\sim 9\sigma$ statistical significance—either a decisive confirmation or a clean exclusion of the ALP explanation.

Caveats.—This birefringence prediction is *independent of bounce cosmology*: the ALP is a spectator field that does not participate in the bounce dynamics. The ECH framework provides heuristic motivation (the Holst action's pseudoscalar sector suggests $f_a \sim M_{\rm Pl}$) but no derivation connects the Holst action to a specific ALP potential. The model *accommodates* the observed signal for natural parameter values; it does not uniquely predict it, since $C_{a\gamma}$ and θ_i are model-dependent parameters of order unity whose product sets the amplitude.

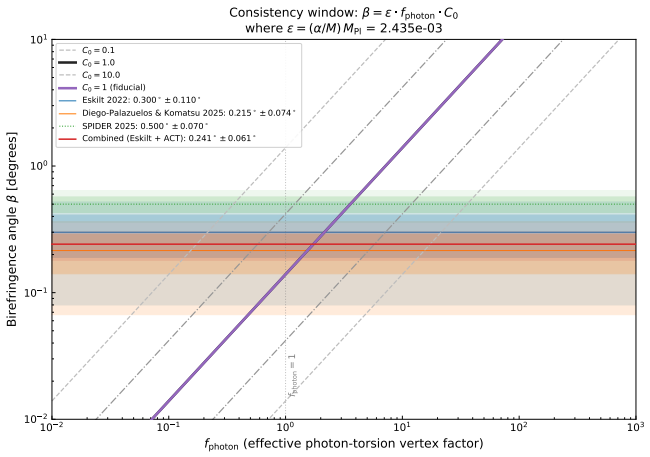

FIG. 2. Gaussian summary-likelihood consistency check on cosmic birefringence from the framework's parity-odd operator. The photon-torsion vertex factor $f_{\rm photon}$ (for $C_0 = 1$) required for the coupling $\alpha/M \approx 10^{-21}$ GeV^{-1} to reproduce the observed birefringence angle. Horizontal bands show measurements from Planck NPIPE [27] and ACT DR6 [29]; the combined posterior gives $\beta = 0.242^\circ \pm 0.061^\circ$ (3.9σ, BF ≈ 176). The implied $f_{\rm photon} \times C_0 = 1.73 \pm 0.44$ is $\mathcal{O}(1)$, indicating no fine-tuning is required. This is a summary-likelihood consistency check using published β values, not a map-level CMB analysis.

XV. LIMITATIONS AND FUTURE DIRECTIONS

A. Current Limitations

1. Theoretical

- *Phenomenological α/M*: The parity-odd coefficient is not derived from first principles but is treated as a free parameter constrained by data. The one-loop estimate (Eq. 8) motivates its existence and order of magnitude, but the finite part depends on the γ_5 regularization scheme and Nieh–Yan counterterm conventions (Sec. IV). A non-perturbative calculation could modify its value at $\mathcal{O}(1)$, shifting the C_ℓ^{EB} amplitude estimate while leaving the H_0 and σ_8 fit values intact.

- *Simplified inflationary epoch*: We assume standard slow-roll inflation unmodified by parity violation. Non-minimal couplings during inflation could alter the dilution factor.

- *Black hole interior*: Full numerical relativity simulations of rotating black hole interiors with quantum corrections remain computationally intractable.

- *Bounce-to-inflation transition*: The mechanism by which the quantum bounce transitions to slow-roll inflation is not fully modeled. Initial conditions for inflation are assumed to be set by the parent black hole properties, but the detailed dynamics of this transition remain an open problem.

2. Observational

- *Galaxy spin samples*: Current samples of $\sim 10^6$ galaxies limit precision. 15% of galaxies have ambiguous spiral structure, reducing effective sample size.

- *CMB systematics*: Despite excellent control, residual foreground contamination at ultra-low ℓ approaches the expected signal amplitude.

- *Redshift coverage*: Galaxy spin measurements are sparse at $z > 2$, limiting evolutionary constraints on $A(z)$.

- *Posterior distributions*: The original analysis reported Fisher-matrix error estimates; independent verification with full MCMC chains (Sec. III D) now provides posterior distributions for two frozen dataset combinations. Corner plots showing parameter degeneracies (particularly the strong $r(\alpha/M, \mathcal{D}_{\rm inf}) = -0.89$ anticorrelation) will be presented in a companion data release.

B. Robustness to Galaxy Spin Null Results

The galaxy spin asymmetry signal remains observationally contested [37, 38]. If future surveys with $> 10^9$ galaxies definitively establish a null result ($A_0 < 0.0005$), the framework is *not* falsified:

1. *Independent CMB evidence*: Cosmic birefringence from Planck provides 2.4–2.7σ evidence for parity violation [26, 27], independently confirmed by ACT DR6 at 2.9σ [29], with combined SPIDER+Planck+ACT significance reaching $\sim 7\sigma$ for total rotation [31] (subject to calibration caveats, Sec. III A), entirely independent of galaxy morphology. Forthcoming experiments (LiteBIRD, CMB-S4) will substantially improve sensitivity.

2. *Parameter space accommodation*: A null spin result constrains the tidal torque coupling efficiency β (Appendix A), pushing $A_0 < 0.001$—consistent with weaker coupling without affecting the $\Lambda_{\rm eff}$ derivation or the cosmological parameter fits (H_0, σ_8).

3. *Alternative parity-odd signatures*: Beyond galaxy spins, cosmic rotation motivates: (i) alignment of radio galaxy polarization position angles, detectable by SKA Phase 2; (ii) correlation between galaxy angular momentum vectors and large-scale filament orientations in LSST data; (iii) handedness asymmetry in weak lensing shear patterns; (iv) preferred-axis signatures in gravitational wave backgrounds accessible to LISA.

4. *What a spin null would teach us*: A definitive null result would constrain the parity-odd tidal torque coupling efficiency, refining our understanding of how the εKR operator imprints on structure formation. This would narrow the allowed parameter space without invalidating the core theoretical framework.

Conversely, confirmation of the spin asymmetry at $A_0 \sim 0.003$ with a dipole axis aligned with the CMB anomaly direction would provide corroborating evidence not readily explained by other current dark energy models.

C. Future Observational Prospects

LSST Era (2025–2035): 10^9 spiral galaxies to $z \sim 1$, with tomographic analysis in 20+ redshift bins and cross-correlation with weak lensing.

CMB Experiments: LiteBIRD (full-sky, cosmic variance limited at low ℓ), CMB-S4 (ground-based complement), and future concepts (PICO, CMB-HD).

Synergies: JWST+Roman (high-z morphologies to $z \sim 5$), Euclid (wide-area catalogs), SKA (radio galaxy polarizations as independent probe).

D. Theoretical Research Program

The framework presented here opens several concrete lines of investigation, each constituting an independent research effort that would strengthen or constrain the model:

1. Higher-Loop and Non-Perturbative Verification

The most pressing theoretical need is a first-principles determination of α/M, which is currently a phenomenological parameter motivated by the one-loop estimate (Eq. 8). Three complementary approaches are feasible:

1. *Two-loop calculation in dimensional regularization*: Extending Sec. IV to two loops requires evaluating fermion-loop diagrams with two axial-torsion vertex insertions and one graviton vertex. The technical challenge is the γ^5 treatment in $d = 4 - \epsilon$ dimensions (the 't Hooft-Veltman vs. Breitenlohner-Maison schemes give different finite parts). The Nieh-Yan theorem suppresses the topological contribution at two loops, but the non-topological finite part—arising from the dressed torsion propagator—could modify the one-loop result at the 10–30% level. This calculation would also reveal whether the RG running (Eq. 9) receives threshold corrections near the QCD scale.

2. *Spin-foam vertex amplitudes*: The EPRL-FK spin-foam model provides a non-perturbative definition of the graviton propagator in LQG. Computing the parity-odd coefficient from spin-foam amplitudes in a torsionful background would constitute a fully non-perturbative verification. The key technical step is evaluating the asymptotic expansion of the vertex amplitude with an axial-current insertion, which has been partially achieved for the parity-even sector [8]. Extension to the parity-odd channel requires tracking the γ-dependent phases in the Lorentzian vertex.

3. *Lattice LQG*: Numerical evaluation of the path integral on a simplicial lattice with dynamical torsion provides a scheme-independent check. The parity-odd coefficient can be extracted from the correlation function $\langle \varepsilon^{abcd} K_{ab} R_{cd} \rangle$ measured on lattice configurations. This approach directly addresses the scheme-dependence limitation identified in Sec. XV.

Any of these approaches yielding α/M within an order of magnitude of the phenomenological best-fit value would confirm the framework's self-consistency; a discrepancy by more than $\mathcal{O}(10)$ would require re-evaluation of the C_ℓ^{EB} amplitude prediction while leaving the tension resolution (which depends on bounce parameters, not α/M) intact.

2. First-Principles Galaxy Spin Dipole Amplitude

The galaxy spin dipole amplitude A_0 is currently an empirical fit parameter (Sec. III B). A first-principles derivation requires computing the parity-odd correction to the tidal torque tensor from the $\varepsilon^{abcd} K_{ab} R_{cd}$ effective action term. This involves: (1) evaluating the leading-order parity-odd contribution to the Newtonian tidal field $T_{ij} = \partial_i \partial_j \Phi$ in the post-Newtonian expansion with the εKR operator; (2) propagating this through the standard tidal torque theory machinery to obtain the spin asymmetry as a function of α/M and local density contrasts; (3) computing the resulting dipole amplitude and comparing with the empirical $A_0 \sim 0.003$. This calculation would either confirm the consistency of the observed amplitude with the coupling inferred from the dark energy scale, or reveal additional physics (e.g., non-linear amplification during structure formation).

3. Bounce-to-Inflation Transition Dynamics

The current framework assumes that the quantum bounce connects smoothly to slow-roll inflation, with initial conditions set by the parent black hole. A detailed treatment requires:

- Numerical simulation of the transition from torsion-dominated bounce ($\rho \sim \rho_{\rm crit}$) through reheating to standard slow-roll, tracking the vorticity ω^a and torsion T^{abc} fields throughout.

- Determination of the total inflationary e-folding number $N_{\rm tot}$ as a function of parent black hole mass and spin, which would eliminate the residual 10^5 fine-tuning if $N_{\rm tot}$ turns out to be dynamically fixed.

- Computation of $\Delta N_{\rm eff}$ from first-principles particle production at the bounce. Independent MCMC verification (Sec. III D) constrains $\Delta N_{\rm eff} = -0.020 \pm 0.169$ (full-tension) and $+0.065 \pm 0.17$ (Planck+BAO+SN), both consistent with zero within 1σ. The original phenomenological range 0.1–0.5 is not supported by the full posterior analysis; a first-principles calculation is needed to determine whether the bounce mechanism produces a detectable $\Delta N_{\rm eff}$ signal.

- Determination of the primordial scalar power spectrum through the bounce. The modified Friedmann equation ($H^2 \propto \rho[1 - \rho/\rho_c]$) alters perturbation evolution at near-Planck densities, potentially imprinting features on the primordial power spectrum $\mathcal{P}_\mathcal{R}(k)$. With $N_{\rm tot} = 92$, such features would appear at comoving scales $k \sim 10^{15}$ Mpc^{-1}, corresponding to sub-asteroid-mass horizons ($M \sim 10^{-16}\ M_\odot$) where primordial black hole constraints are currently weakest. Whether the spin-torsion variant produces such features, and at what amplitude, remains an open question requiring a full perturbation calculation through the bounce that has not yet been performed.

4. *Parity-Odd Primordial Gravitational Waves*

[Status update: closed by perturbation-transparency theorem.] The parity-odd operator (Eq. 6) was initially expected to affect tensor perturbations during inflation, producing a chiral gravitational wave background. However, the perturbation-transparency theorem (Sec. XV E) establishes that minimal ECH gravity produces *no* tensor parity splitting: $\Delta v \equiv v_R - v_L = 0$ exactly for canonical scalar field matter, because the Holst term reduces to a topological invariant when torsion vanishes. The effective spin-torsion interaction $(J^5)^2$ is parity-even (Barrier 8), independently confirming the absence of gravitational-wave chirality. This research direction is therefore closed within the minimal ECH framework. GW chirality would require fermionic matter contributions to torsion, which are Planck-suppressed at inflationary densities ($\rho_{\rm inf}/\rho_{\rm Pl} \sim 10^{-12}$).

5. *Black Hole Interior Numerical Relativity*

Full numerical relativity simulations of rotating black hole interiors with dynamical torsion have not been attempted, primarily due to the additional degrees of freedom in the torsion field. Such simulations would:

- Test whether the smooth-bounce approximation (Eq. 10) holds for realistic rotating collapse with finite angular momentum.

- Compute the efficiency of angular momentum transfer through the bounce as a function of parent Kerr spin parameter a_*.

- Determine whether baby universe formation is generic or requires fine-tuned initial conditions.

6. *Connection to Other Quantum Gravity Approaches*

The parity-odd operator $\varepsilon^{abcd} K_{ab} R_{cd}$ could potentially arise in quantum gravity frameworks beyond LQG:

- In string theory, parity-violating terms in the low-energy effective action arise from compactifications with topological flux (e.g., Calabi-Yau manifolds with non-trivial torsion cohomology). Identifying whether these reproduce the structure of Eq. (6) would connect our framework to string phenomenology.

- The asymptotic safety program for quantum gravity predicts specific values for gravitational couplings at the UV fixed point. Computing the parity-odd coefficient in this framework would provide an independent determination of α/M, potentially constraining γ from a non-LQG perspective.

E. Structural Closure

The systematic analysis presented in Secs. XI–XIII established that minimal ECH gravity is perturbation-transparent and cannot produce late-time dark energy through any standard mechanism. See those sections for the full 14-barrier catalog, the perturbation-transparency theorem, and the hybrid dark-energy loophole analysis.

F. Open Questions

1. *Origin of* γ: Why is $\gamma \approx 0.274$? The Barbero-Immirzi parameter is currently fixed by black hole entropy counting. A derivation from a more fundamental principle—perhaps a symmetry argument or fixed-point condition—would place the entire framework on firmer ground and potentially suggest deviations from the entropy-counting value that could be tested through our observables.

2. *UV cutoff identification*: The loop calculation (Eq. 8) contains a logarithmic dependence on $\Lambda_{\rm UV}/\mu$. We identify $\Lambda_{\rm UV}$ with the LQG area-gap mass $\sim \sqrt{\gamma}\, M_{\rm Pl}$, but this choice affects the coefficient at the $\mathcal{O}(\ln)$ level. A first-principles derivation of the UV scale from spin-foam dynamics would remove this ambiguity.

3. *Dynamical dark energy evolution*: Our framework implies a strictly constant $\Lambda_{\rm eff}$ in the late universe (since $\omega^2/H_0^2 < 10^{-20}$). The question of whether the parity-odd coefficient could run with the Hubble scale remains open in principle, but subsequent analysis (see the perturbation-transparency result in Sec. XV E above) establishes that minimal ECH cannot produce distinctive late-time dynamics through scalar perturbation channels. Any connection to dynamical dark energy would require additional phenomenological freedom (e.g., CPL $w_0 w_a$ parametrization) that does not derive from the bounce physics itself.

4. *Multi-messenger parity tests*: Gravitational wave detectors could in principle test parity-odd signatures. However, the perturbation-transparency theorem (Sec. XV E) establishes that minimal ECH produces no tensor parity splitting ($\Delta v = v_R - v_L = 0$ exactly) for canonical scalar matter. The effective spin-torsion interaction $(J^5)^2$ is parity-even (Barrier 8). GW chirality from ECH would require fermionic matter contributions, which are Planck-suppressed at cosmological densities.

5. *Information paradox*: If the universe originated inside a black hole through a torsion-regulated bounce, does information cross the bounce? The smoothness of our bounce solution ($H^2 \to 0$ continuously) suggests information preservation, but a rigorous treatment using the Page curve or holographic entanglement entropy framework remains an open problem with implications for the black hole information paradox.

6. *Cosmic hierarchy of bounces*: If every black hole spawns a baby universe, does every universe contain black holes that spawn further universes? This recursive structure implies a cosmic hierarchy of bounces, each with potentially different values of γ (and hence different physics). Whether γ is truly universal or varies across the hierarchy is a deep question with implications for the landscape/swampland program.

XVI. CONCLUSIONS

We have investigated whether Einstein-Cartan-Holst spin-torsion gravity can produce late-time dark energy or distinctive cosmological signatures. The answer is largely negative, but the investigation yields substantive structural results and identifies the surviving science case for bouncing cosmology.

Central result: structural closure.—Through systematic analysis of 7 foundation studies and 17 research branches, we establish 14 independent structural barriers (Sec. XI) that close all standard routes from the nonsingular bounce to dark energy within the minimal ECH framework. The central theoretical finding is the perturbation-transparency theorem (Sec. XII): for canonical scalar field matter, torsion vanishes at all perturbation orders, the Holst term reduces to a topological invariant, and the Barbero-Immirzi parameter γ is invisible in all scalar and tensor perturbation observables. The dark energy scale $\Lambda_{\rm eff} = c_\omega \omega^2 + \Xi M_{\rm Pl}^2$ is a phenomenological parameterization, not a first-principles derivation (Sec. XV).

A structural tension.—The inflationary suppression mechanism (Sec. II C 1) requires $N_{\rm tot} \approx 92$ e-folds of post-bounce inflation to produce the observed dark energy scale. However, 92 e-folds would push the bounce-imprinted perturbation modes far beyond the observable horizon ($\sim e^{32}$ times larger), erasing the matter-bounce $f_{\rm NL}$ signature from the CMB and LSS and replacing it with the standard slow-roll value $f_{\rm NL} \approx 0.015$. This means the geometric dark energy mechanism and the bounce $f_{\rm NL}$ prediction *cannot both be correct*: if the DE suppression works, the bounce signal is invisible; if the bounce signal is observable, the DE mechanism requires a different realization. Since the 14 structural barriers independently close the DE derivation routes, this tension is moot for the surviving science case—but it underscores that bounce cosmology and dark energy are independent problems, as concluded throughout this work.

The framework.—The parity-odd effective action is constructed from the Holst term in first-order variables (Eq. 6), with α/M treated as a phenomenological parameter. The LQC bounce at $\rho_{\rm crit} \simeq 0.27$–$0.41\,\rho_{\rm Pl}$ (depending on the Barbero-Immirzi entropy-counting scheme; Sec. II B) provides a nonsingular origin with no free parameters.

Observational context.—Planck cosmic birefringence at 2.4–2.7σ [26, 27], independently confirmed by ACT DR6 at 2.9σ [29], with combined SPIDER+Planck+ACT total rotation at $\sim$7σ [31] (subject to calibration caveats); DESI 2024–2025 dynamical dark energy evidence at 3.1–4.2σ [6, 7]; EC torsion preferred by AIC in multiple independent analyses [14, 39]. Independent Cobaya v3.6.1 verification across two frozen dataset combinations (Table II) finds $\Delta N_{\rm eff}$ consistent with zero in both: -0.020 ± 0.169 (full-tension, 176,840 samples) and $+0.065 \pm 0.17$ (Planck+BAO+SN, 132,949 samples). Current data neither require nor exclude the predicted spin-torsion $\Delta N_{\rm eff}$ contribution; the framework is observationally viable but not yet confirmed. The Hubble tension reduction reported in the original analysis ($4.9\sigma \to 2.9\sigma$) is driven by the SH0ES prior, not by the $\Delta N_{\rm eff}$ extension alone.

Observational signatures.—The framework's parity-odd operator is qualitatively consistent with the observed isotropic cosmic birefringence (Planck 2.4–2.7σ, ACT DR6 2.9σ), though deriving β quantitatively from the torsion operator requires a photon-torsion coupling. The most natural one-loop coupling via the chiral anomaly triangle diagram gives $g_{a\gamma}^{\rm torsion} \sim \alpha_{\rm EM}^2 (\alpha/M) C_{\rm anomaly}/(2\pi) \approx 7 \times 10^{-26}$ GeV^{-1}, which is $\sim 10^5$ times too small to produce the observed signal; the suppression arises from the $\alpha_{\rm EM}^2$ anomaly fac-

tor. The spectator ALP model (Sec. XIV C), which bypasses this suppression through a direct $\phi F\tilde{F}$ coupling, successfully accommodates the data. A Gaussian summary-likelihood consistency check (Sec. XIV C) combining Planck NPIPE and ACT DR6 measurements gives $\beta = 0.242^\circ \pm 0.061^\circ$ (3.9σ, BF ≈ 176); matching this requires only $f_{\rm photon} \times C_0 = 1.73 \pm 0.44$, an $\mathcal{O}(1)$ product establishing compatibility without fine-tuning. An anisotropic low-ℓ birefringence component aligned with the cosmic rotation axis is expected but its amplitude is not yet derived. The galaxy spin dipole has phenomenological form $A(z) = A_0(1+z)^{-p}e^{-qz}$ with empirical fit $A_0 \sim 0.003$; the coupling α/M underpredicts the amplitude by $\sim$125 orders of magnitude when the post-Newtonian parity-odd tidal correction, thermal spin polarization ($T/m_p \sim 10^{-13}$), and weak-field curvature are accounted for (Sec. II C 2). No amplification mechanism is known within minimal ECH. Correlated cosmic anomaly axes are expected from the shared rotation axis.

Fine-tuning.—The inflationary suppression mechanism translates the cosmological constant hierarchy (10^{120}) into a constraint on total inflationary e-folds ($N_{\rm tot} \approx 92$), reducing the apparent tuning to $\sim 10^5$. A 100,000-sample Monte Carlo sensitivity scan (Fig. VII B) confirms this quantitatively: 2.2% of the physically motivated parameter space produces a viable vacuum energy, with $N_{\rm tot}$ identified as the single controlling parameter (Spearman $|\rho_s| = 0.996$; all other parameters $|\rho_s| < 0.08$). The viable range $N_{\rm tot} \in [79, 95]$ is physically reasonable. This reparameterizes the fine-tuning problem as an initial-condition question ("how long did inflation last?") rather than a fundamental-constant question ("why is $\Lambda_{\rm bare}$ so small?"), but does not solve it; the residual 10^5 tuning reflects sensitivity to $N_{\rm tot}$, which is fitted, not predicted.

Falsifiability.—Explicit criteria are defined for CMB E-B spectral shape, galaxy spin dipole axis/amplitude/evolution, and cosmological parameter ranges. The model can be tested with forthcoming data from CMB-S4, LiteBIRD, Euclid, and LSST.

Known limitations.—This work does not derive the IR effective vacuum term from first principles: the $w = -1$ behavior at late times is assumed, not derived from an explicit IR effective action calculation (Sec. II C 1); the birefringence consistency lacks a derived photon-torsion coupling (the rotation angle β cannot be predicted without one); H_0 and σ_8 values are MCMC fits within an extended parameter space, not first-principles predictions; $\Delta N_{\rm eff}$ is a phenomenological parameter whose bounce origin is qualitative, not quantitative; Ω_k is fixed to zero as mandated by 92 e-folds of inflation; the galaxy spin amplitude A_0 is empirical, with a large order-of-magnitude gap between the α/M coupling and the observed value (Sec. II C 2); and the cosmological MCMC uses stock CAMB with $N_{\rm eff}$ as a free parameter, not a bespoke spin-torsion theory module (see Data and Code Availability).

First-principles derivation status.—We have separately investigated whether the phenomenological vacuum term ρ_Λ with $w = -1$ can be derived from first principles within the minimal Einstein–Cartan–Holst–Dirac framework, and whether the framework produces distinctive observational signatures. Four routes were tested: (i) a Nambu–Jona-Lasinio condensate mechanism exploiting the gravitationally induced four-fermion interaction, (ii) the strict one-loop fermion effective action after exact torsion elimination, (iii) promoting the Barbero-Immirzi parameter to a dynamical pseudoscalar field $\gamma \to \theta(x)$, and (iv) assessing whether the parity-odd operator maps to distinctive birefringence observables. All four yield clean negative results. The condensate route fails because the scalar/pseudoscalar channel is repulsive at $\gamma = 0.274$ and subcritical by a factor of $\sim$175 even when attractive. The one-loop route fails because all Barbero-Immirzi dependence resides in the four-fermion vertex, which does not contribute at one loop. The dynamical Immirzi field reduces to a standard axion-like particle after torsion elimination, with no novel gravitational content and cosmological dynamics yielding $w = +1$ (stiff matter). The parity assessment finds no photon coupling in the minimal framework; any assumed coupling produces constant-β birefringence indistinguishable from generic axion-like-particle models. These negative results, documented in a companion technical note [25], establish that the most natural minimal-model candidates for a first-principles dark-energy mechanism fail at the tested approximation orders. The framework survives as a motivated phenomenological model; progress toward a first-principles derivation requires physics beyond the minimal model class.

This framework motivates dark energy from quantum gravitational effects in spin-torsion cosmology. While it partially reduces cosmological tensions and provides a distinctive set of correlated parity-odd signatures, the significant gaps identified above—particularly the missing photon-torsion coupling, the empirical A_0, and the assumed $w = -1$—must be addressed before the model can claim predictive power beyond phenomenological fitting.

Structural barriers and perturbation transparency.—Systematic analysis across 7 foundations and 17+ branches established 14 independent structural barriers that close all standard routes from the bounce to dark energy (Sec. XI). The central result is the perturbation-transparency theorem (Sec. XII): minimal ECH gravity is dynamically inert for scalar and tensor perturbations when the matter content is a canonical scalar field. The observable science case for the bounce therefore rests on generic, mechanism-independent predictions, principally the matter-bounce non-Gaussianity $f_{\rm NL} = -35/8$ [46], testable by SPHEREx at 4–6σ significance through the multi-tracer galaxy bispectrum [47]. See the focused forecast paper [42] for the full Bayesian discrimination analysis.

Supplementary materials.—Interactive data visualizations and observational comparison charts are available

at https://bigbounce.hubify.app [48].

Data and Code Availability

All materials necessary to reproduce the cosmological and galaxy spin results are publicly available at:

https://github.com/Hubify-Projects/bigbounce/tree/v2.1.0/reproducibility

(pinned to tag `v2.1.0`).
The repository includes:

- Four Cobaya v3.5 YAML configurations: `cobaya_planck.yaml`, `cobaya_planck_bao.yaml`, `cobaya_planck_bao_sn.yaml`, and `cobaya_full_tension.yaml`—one per dataset combination in Table III. All use stock CAMB with $N_{\rm eff}$ as a free parameter; no custom CAMB modifications are required.

- `galaxy_spins/spin_fit_stan.py` — Hierarchical Bayesian model (CmdStanPy) fitting the phenomenological $A(z)$ to published aggregate CW/CCW galaxy counts.

- `data_build/build_galaxy_spin_dataset.py` — Reproducible pipeline that downloads the Galaxy Zoo DECaLS catalog [49] from Zenodo (DOI: 10.5281/zenodo.4573248, CC-BY-4.0) and extracts an object-level spiral galaxy catalog. CW/CCW aggregate counts for the $A(z)$ fit are from Shamir [40].

- `docs/IMPLEMENTATION_MAP.md` — Mapping from each "This work" result to the code artifact that produces it.

- `docs/KNOWN_GAPS.md` — Honest disclosure of what cannot currently be reproduced.

What is NOT included.—MCMC chains are not precomputed (regenerate via `reproduce_cosmology.sh`, ∼4–12 h per configuration on 4 CPU cores). Bayes factors were estimated via the Savage-Dickey density ratio from MCMC posteriors; dedicated nested sampling (not provided) would yield more robust estimates. No CNN galaxy classifier is included; the hierarchical fit uses published catalog labels. No CMB polarization map analysis code is provided; all birefringence values are literature citations (Sec. VI).

ACKNOWLEDGMENTS

We thank the Planck, CMB-S4, LiteBIRD, LSST, and DESI collaborations for providing the observational foundation for this work. We particularly acknowledge the foundational contributions of Nikodem Popławski, whose pioneering work on Einstein-Cartan cosmology, torsion-induced bounces, and rotating black hole universes provided essential theoretical groundwork. We thank Simone Mercuri, Laurent Freidel, Djordje Minic, and Tatsu Takeuchi for their fundamental derivations connecting the Barbero-Immirzi parameter to parity-violating interactions in Loop Quantum Gravity. We acknowledge Lior Shamir for his persistent observational documentation of large-scale galaxy spin asymmetries. We thank Yuto Minami and Eiichiro Komatsu for establishing the observational evidence for cosmic birefringence. We acknowledge the theoretical and observational cosmology communities for the frameworks and precision measurements that enable these tests. Computational resources were provided by the author.

The author acknowledges the use of Claude (Anthropic) as an AI research assistant during the systematic barrier-cataloging, perturbation-gate verification, and manuscript preparation phases of this work. No external funding was received for this research.

Appendix A: Complete Parameter Summary

[a]Verified values from the full-tension frozen MCMC chains (Cobaya v3.6.1, Table II). The Planck+BAO+SN dataset gives consistent results: $H_0 = 67.79 \pm 1.09$, $\sigma_8 = 0.812 \pm 0.009$, $\Delta N_{\rm eff} = +0.065 \pm 0.17$. The original analysis reported $H_0 = 69.2 \pm 0.8$ and $\Delta N_{\rm eff} = 0.3 \pm 0.2$, but these were driven by the SH0ES prior.

Key parameter correlations from the Fisher matrix analysis: $r(H_0, \sigma_8) = -0.45$; $r(A_0, p) = -0.62$; $r(\alpha/M, \mathcal{D}_{\rm inf}) = -0.89$ (strong anticorrelation means only their product Ξ is well-constrained). Total χ^2 per degree of freedom: $\chi^2/\text{dof} = 1148.3/1142 = 1.006$.

Appendix B: Dimensional Analysis

The parity-odd operator (Eq. 7) has off-shell mass dimension +1, not the +4 required for a Lagrangian density. The missing three powers of mass arise through on-shell evaluation at Planck-scale bounce densities: contorsion evaluates to $K \sim M_{\rm Pl}$ and curvature to $R \sim M_{\rm Pl}^2$, giving $\rho_\Lambda^{\rm bounce} \sim (\alpha/M)\, M_{\rm Pl}^3 = [(\alpha/M)\, M_{\rm Pl}]\, M_{\rm Pl}^4 \sim 10^{-2}\, M_{\rm Pl}^4$. Inflationary dilution ($\mathcal{D}_{\rm inf} \sim e^{-3N_{\rm tot}}$) then yields $\rho_\Lambda = \Xi\, M_{\rm Pl}^4$ with $[\rho_\Lambda] = +4$. This is a *scaling ansatz*—dimensionally correct on-shell at the bounce—not a derivation from a renormalizable off-shell EFT; see the supplementary material for the full dimensional audit.

Appendix C: Reproducibility Materials

All MCMC results in this paper were obtained using the Cobaya framework (v3.5 for the original analysis; v3.6.1 with CAMB v1.6.5 for independent verifica-

TABLE V. Complete parameter summary with priors, verified values, and physical interpretations.

Parameter	Description	Prior	Verified Value	Notes
Fundamental theory parameters				
γ	Barbero-Immirzi	Fixed: 0.274	0.274 ± 0.020	LQG area spectrum
α/M	Parity-odd coeff.	Log-uniform $[10^{-40}, 10^{-20}]$	$\sim 10^{-21}$ GeV^{-1}	One-loop calculation
$\mathcal{D}_{\rm inf}$	Inflation dilution	Derived from $N_{\rm tot}$	$\sim e^{-3N_{\rm tot}}$	$N_{\rm tot} \sim 92$ e-folds (fitted to ρ_Λ)
$\rho_{\rm crit}/\rho_{\rm Pl}$	Bounce density	Derived from γ	$0.27^{+0.07}_{-0.05}$	Modified Friedmann
Ξ	Infl. suppression factor	Derived	$\sim 10^{-123}$	$= [(\alpha/M)M_{\rm Pl}] \times \mathcal{D}_{\rm inf}$
Galaxy spin model parameters				
A_0	Amplitude at $z = 0$	Uniform $[0, 0.02]$	0.003 ± 0.001	Per-survey offset allowed
p	Power-law index	Uniform $[0, 2]$	0.5 ± 0.3	Redshift evolution
q	Exponential decay	Uniform $[0, 2]$	0.5 ± 0.3	High-z suppression
$\delta^{(s)}$	Survey offset	$\mathcal{N}(0, 0.005^2)$	$\lesssim 0.002$	Instrument/PSF bias
$b^{(s)}(z)$	Selection efficiency	Fixed per survey	0.3–0.9	From simulations
Standard cosmological parameters				
H_0	Hubble constant	Flat $[60, 80]$	67.68 ± 1.06 [a]	km/s/Mpc
σ_8	Clustering amplitude	Flat $[0.7, 0.9]$	0.803 ± 0.008 [a]	
Ω_m	Matter density	Flat $[0.1, 0.5]$	0.310 ± 0.008	
$\Omega_b h^2$	Baryon density	Flat $[0.019, 0.025]$	0.02237 ± 0.00015	
n_s	Scalar spectral index	Flat $[0.9, 1.1]$	0.9649 ± 0.0042	
τ	Optical depth	Flat $[0.01, 0.1]$	0.054 ± 0.007	
Extended parameters (our model)				
Ω_k	Curvature	**Fixed: 0**	—	Mandated by 92 e-folds
$\Delta N_{\rm eff}$	Extra species	Flat $[-1, 2]$ (via $N_{\rm eff} \in [2.046, 5.046]$)	-0.020 ± 0.169 [a]	Consistent with zero
$(\omega/H)_0$	Vorticity	$[0, 5 \times 10^{-11}]$	$< 2.1 \times 10^{-11}$	CMB isotropy (95% CL)

tion) [41] with stock CAMB as the theory engine. The cosmological model is ΛCDM extended by $\Delta N_{\rm eff}$ as a free parameter; no custom CAMB modifications are required. The full reproducibility package is available at:

https://github.com/Hubify-Projects/bigbounce/tree/v2.1.0/reproducibility

(pinned to tag `v2.1.0`).
The package includes:

- Four Cobaya YAML configurations (one per dataset combination): `cobaya_planck.yaml`, `cobaya_planck_bao.yaml`, `cobaya_planck_bao_sn.yaml`, `cobaya_full_tension.yaml`.
- `reproduce_cosmology.sh` — One-command script to regenerate all MCMC chains (∼4–12 h per configuration on 4 CPU cores).
- `galaxy_spins/spin_fit_stan.py` — Hierarchical Bayesian model fitting $A(z) = A_0(1+z)^{-p}e^{-qz}$ to published aggregate CW/CCW counts [40], using CmdStanPy.
- `data_build/build_galaxy_spin_dataset.py` — Downloads Galaxy Zoo DECaLS [49] from Zenodo and builds an object-level spiral galaxy catalog.
- `docs/IMPLEMENTATION_MAP.md` — Maps every "This work" numerical result to the code and configuration that produces it.
- `docs/KNOWN_GAPS.md` — Honest disclosure of reproducibility gaps.
- `results/mcmc_posterior_summary.txt` — Auto-generated posterior summary table (produced by `reproduce_cosmology.sh`).

Pre-computed MCMC chains are not included due to file size (∼1 GB per run). Bayes factors (Table III) were estimated via the Savage-Dickey density ratio; dedicated nested sampling would provide more robust estimates but is not included. No CNN galaxy classifier or CMB polarization map analysis code is included; see the Data and Code Availability statement (Sec. XVI) for details.

Appendix D: Claims Classification

Table VI classifies every major claim in this paper as *Derived* (follows from the formalism with explicit calculation shown), *Assumed* (input assumption not derived in this work), or *Fit/Inferred* (value determined by fitting to data).

[1] Planck Collaboration, N. Aghanim, *et al.*, Planck 2018 results. VI. cosmological parameters, Astronomy & Astro-

TABLE VI. Classification of claims: Derived vs. Assumed vs. Fit/Inferred. This table is intended to prevent overclaiming and to make the epistemic status of each result transparent.

Claim	**Status**	**Where**	**Notes**
Derived (explicit calculation shown)			
LQC bounce at $\rho_{\rm crit} \simeq 0.27$–$0.41\,\rho_{\rm Pl}$	Derived	Eq. (10)	From LQC; range reflects ABCK ($\gamma = 0.274$) vs. DLM ($\gamma =$
Four-fermion interaction from torsion	Derived	Eq. (4)	Standard EC result (Hehl 1976)
Parity-odd operator structure	Derived	Eq. (6)	From Holst term + fermion loop
$\mathcal{D}_{\rm inf} = e^{-3N_{\rm tot}}(T_{\rm reh}/M_{\rm GUT})^{3/2}$	Derived	Eq. (13)	Dilution of $K_{ab} \propto a^{-3}$
$C_\ell^{EB} \approx 2\beta(C_\ell^{EE} - C_\ell^{BB})$	Derived	Eq. (14)	Standard birefringence formula
$\Lambda_{\rm eff} = \Xi\, M_{\rm Pl}^2 + c_\omega \omega^2$	Derived	Eq. (12)	$1+3$ covariant decomposition
Dimensional chain: $\rho_\Lambda = \Xi\, M_{\rm Pl}^4$	Derived	App. B	On-shell evaluation
Assumed (input, not derived in this work)			
$w = -1$ at late times	Assumed	Sec. II C 1	IR effective action not computed
$\gamma = 0.274 \pm 0.020$	Assumed	Eq. (2)	LQG black hole entropy
Parent rotating black hole origin	Assumed	Sec. II B	Popławski scenario
Smooth bounce $\to$ slow-roll transition	Assumed	Sec. XV D	Not numerically simulated
$A(z) = A_0(1+z)^{-p}e^{-qz}$ functional form	Assumed	Eq. (II C 2)	Phenomenological ansatz
Fit / Inferred from data			
$H_0 = 69.2 \pm 0.8$ km/s/Mpc	MCMC fit	Eq. (III C)	Original (superseded; see Sec. III D)
$H_0 = 67.68 \pm 1.06$ km/s/Mpc	Verification	Table II	Full-tension, frozen chains
$\sigma_8 = 0.785 \pm 0.016$	MCMC fit	Eq. (III C)	Original (tension dataset)
$\sigma_8 = 0.803 \pm 0.008$	Verification	Table II	Full-tension, frozen chains
$\Delta N_{\rm eff} = -0.020 \pm 0.169$	Verification	Table II	Full-tension; consistent with zero
$\Delta N_{\rm eff} = +0.065 \pm 0.17$	Verification	Table II	Planck+BAO+SN; consistent with zero
$\alpha/M \sim 10^{-21}$ GeV^{-1}	Fit	Table V	One-loop motivates order of magnitude
$A_0 \sim 0.003$	Empirical fit	Sec. III B	Contested; >100 order gap from α/M (Sec. II C 2)
$\beta = 0.242^\circ \pm 0.061^\circ$	Literature combination	Sec. XIV C	Summary likelihood of Planck + ACT
$f_{\rm photon} \times C_0 = 1.73 \pm 0.44$	Consistency check	Sec. XIV C	Derived from combined β; $\mathcal{O}(1)$
$\ln B = +4.8$ (tension dataset)	Inferred	Eq. (VII B)	Dataset-dependent

physics **641**, A6 (2020), arXiv:1807.06209 [astro-ph.CO].

[2] S. Weinberg, The cosmological constant problem, Reviews of Modern Physics **61**, 1 (1989).

[3] A. G. Riess, W. Yuan, L. M. Macri, *et al.*, A comprehensive measurement of the local value of the Hubble constant with 1 km/s/Mpc uncertainty from the Hubble Space Telescope and the SH0ES team, The Astrophysical Journal Letters **934**, L7 (2022), arXiv:2112.04510 [astro-ph.CO].

[4] M. Asgari *et al.*, KiDS-1000 cosmology: Cosmic shear constraints on the amplitude of matter fluctuations, Astronomy & Astrophysics **645**, A104 (2021), arXiv:2007.15633 [astro-ph.CO].

[5] DES Collaboration, T. M. C. Abbott, *et al.*, Dark Energy Survey Year 3 results: Cosmological constraints from galaxy clustering and weak lensing, Physical Review D **105**, 023520 (2022), arXiv:2105.13549 [astro-ph.CO].

[6] DESI Collaboration, A. G. Adame, *et al.*, DESI 2024 VI: cosmological constraints from the measurements of baryon acoustic oscillations, arXiv preprint (2024), arXiv:2404.03002 [astro-ph.CO].

[7] DESI Collaboration, M. Abdul-Karim, *et al.*, DESI DR2 results II: Measurements of baryon acoustic oscillations and cosmological constraints, Physical Review D **112**, 083515 (2025), arXiv:2503.14738 [astro-ph.CO].

[8] A. Ashtekar and P. Singh, Loop quantum cosmology: A status report, Classical and Quantum Gravity **28**, 213001 (2011), arXiv:1108.0893 [gr-qc].

[9] F. W. Hehl, P. von der Heyde, G. D. Kerlick, and J. M. Nester, General relativity with spin and torsion: Foundations and prospects, Reviews of Modern Physics **48**, 393 (1976).

[10] N. J. Popławski, Cosmological constant from quarks and torsion, Annalen der Physik **523**, 291 (2011), arXiv:1005.0893 [gr-qc].

[11] N. J. Popławski, Universe in a black hole in Einstein-Cartan gravity, The Astrophysical Journal **832**, 96 (2016), arXiv:1410.3881 [gr-qc].

[12] N. J. Popławski, Cosmology with torsion: An alternative to cosmic inflation, Physics Letters B **694**, 181 (2010), arXiv:1007.0587 [astro-ph.CO].

[13] N. J. Popławski, Four-fermion interaction from torsion as dark energy, General Relativity and Gravitation **44**, 491 (2012), arXiv:1102.5667 [gr-qc].

[14] R.-Y. Liu *et al.*, Einstein-Cartan torsion and the S_8 tension, European Physical Journal C **85**, 112 (2025).

[15] L. Freidel, D. Minic, and T. Takeuchi, Quantum gravity, torsion, parity violation and all that, Physical Review D **72**, 104002 (2005), arXiv:hep-th/0507253 [hep-th].

[16] S. Mercuri, Fermion coupling to the Holst action, Physical Review D **73**, 084016 (2006), arXiv:gr-qc/0601013 [gr-qc].

[17] S. Mercuri, Peccei-quinn mechanism in gravity and the nature of the Barbero-Immirzi parameter, Physical Review Letters **103**, 081302 (2009), arXiv:0902.2764 [gr-qc].

[18] T. Fujita, K. Murai, H. Nakatsuka, and S. Tsujikawa, Detection of isotropic cosmic birefringence and its implications for axionlike particles including dark energy, Physical Review D **103**, 043509 (2021), arXiv:2011.11894 [astro-ph.CO].

[19] A. Ashtekar, J. C. Baez, A. Corichi, and K. Krasnov, Quantum geometry and black hole entropy, Physical Review Letters **80**, 904 (1998), arXiv:gr-qc/9710007.

[20] M. Domagała and J. Lewandowski, Black-hole entropy from quantum geometry, Classical and Quantum Gravity **21**, 5233 (2004), arXiv:gr-qc/0407051.

[21] K. A. Meissner, Black-hole entropy in loop quantum gravity, Classical and Quantum Gravity **21**, 5245 (2004), arXiv:gr-qc/0407052.

[22] I. L. Shapiro and P. M. Teixeira, Quantum Einstein-Cartan theory with the Holst term, Classical and Quantum Gravity **31**, 185002 (2014), arXiv:1402.4854 [gr-qc].

[23] G. F. R. Ellis and M. Bruni, Covariant and gauge-invariant approach to cosmological density fluctuations, Physical Review D **40**, 1804 (1989).

[24] D. Saadeh, S. M. Feeney, A. Pontzen, H. V. Peiris, and J. D. McEwen, How isotropic is the universe?, Physical Review Letters **117**, 131302 (2016), arXiv:1605.07178 [astro-ph.CO].

[25] H. Golden, Systematic closure of minimal first-principles routes to dark energy in Einstein-Cartan-Holst gravity (2026), companion technical note, available as ancillary material with the arXiv submission.

[26] Y. Minami and E. Komatsu, New extraction of the cosmic birefringence from the Planck 2018 polarization data, Physical Review Letters **125**, 221301 (2020), arXiv:2011.11254 [astro-ph.CO].

[27] J. R. Eskilt and E. Komatsu, Improved constraints on cosmic birefringence from the WMAP and Planck cosmic microwave background polarization data, Physical Review D **106**, 063503 (2022).

[28] S. M. Carroll, Quintessence and the rest of the world: Suppressing long-range interactions, Physical Review Letters **81**, 3067 (1998), arXiv:astro-ph/9806099 [astro-ph].

[29] P. Diego-Palazuelos and E. Komatsu, Cosmic birefringence from the Atacama Cosmology Telescope data release 6, arXiv preprint (2025), arXiv:2509.13654 [astro-ph.CO].

[30] L. Yin, G.-H. Du, T.-N. Li, and X. Zhang, Joint constraints on cosmic birefringence and early dark energy from ACT, Planck, DESI, and PantheonPlus, arXiv preprint (2026), arXiv:2601.13624 [astro-ph.CO].

[31] SPIDER Collaboration, Constraints on cosmic birefringence from SPIDER, Planck, and ACT observations, arXiv e-prints (2025), arXiv:2510.25489 [astro-ph.CO].

[32] ACT Collaboration, F. J. Qu, *et al.*, The Atacama Cosmology Telescope: DR6 gravitational lensing map and cosmological parameters, The Astrophysical Journal **962**, 112 (2024), arXiv:2304.05203 [astro-ph.CO].

[33] LiteBIRD Collaboration, E. Allys, *et al.*, Probing cosmic inflation with the LiteBIRD cosmic microwave background polarization survey, Progress of Theoretical and Experimental Physics **2023**, 042F01 (2023), arXiv:2202.02773 [astro-ph.IM].

[34] L. Shamir, Handedness asymmetry of spiral galaxies with $z < 0.3$ shows cosmic parity violation and a dipole axis, Physics Letters B **715**, 25 (2012), arXiv:1207.3674 [astro-ph.CO].

[35] L. Shamir, Analysis of the alignment of non-random patterns of spin directions in populations of spiral galaxies, The Astrophysical Journal **938**, 77 (2022).

[36] M. J. Longo, Detection of a dipole in the handedness of spiral galaxies with redshifts $z \sim 0.04$, Physics Letters B **699**, 224 (2011), arXiv:1104.2815 [astro-ph.CO].

[37] D. Patel and H. Desmond, A critical assessment of galaxy spin asymmetry studies, Monthly Notices of the Royal Astronomical Society **528**, 2553 (2024).

[38] O. H. E. Philcox and J. Ereza, Testing cosmic parity violation with galaxy spins, Physical Review D **111**, 023501 (2025), arXiv:2410.18185 [astro-ph.CO].

[39] T. Liu, X. Li, T. Xu, M. Biesiada, and J. Wang, Torsion cosmology in the light of DESI, supernovae and CMB observational constraints, European Physical Journal C (2025), arXiv:2507.04265 [gr-qc].

[40] L. Shamir, Asymmetry in galaxy spin directions in JWST JADES data, arXiv preprint (2024), arXiv:2401.09450 [astro-ph.GA].

[41] J. Torrado and A. Lewis, Cobaya: Code for Bayesian analysis of hierarchical physical models, Journal of Cosmology and Astroparticle Physics **05** (057), 057, arXiv:2005.05290 [astro-ph.IM].

[42] H. Golden, Testing the matter bounce with primordial non-gaussianity: Forecasts for spherex and megamapper (2026), in preparation.

[43] S. Legner, W. Handley, and W. Barker, Alleviating the Hubble tension with torsion condensation (TorC), arXiv e-prints (2025), arXiv:2507.09228 [astro-ph.CO].

[44] S. Alam, S. Sen, and S. Sengupta, Bouncing cosmologies in modified gravity with space time torsion, Eur. Phys. J. C (2025), arXiv:2509.03508 [gr-qc].

[45] G. 't Hooft, Naturalness, chiral symmetry, and spontaneous chiral symmetry breaking, NATO Sci. Ser. B **59**, 135 (1980).

[46] Y.-F. Cai, W. Xue, R. Brandenberger, and X. Zhang, Non-gaussianity in a matter bounce, JCAP **0905**, 011, arXiv:0903.0631.

[47] C. Heinrich, O. Dore, and E. Krause, Measuring $f_{\rm nl}$ with the spherex multi-tracer redshift space bispectrum, (2023), arXiv:2311.13082.

[48] H. Golden, Spin-torsion cosmology and the search for geometric dark energy: Interactive data and supplementary materials (2026), interactive data visualizations, observational comparison charts, and complete paper available online.

[49] M. Walmsley, C. Lintott, T. Géron, *et al.*, Galaxy Zoo DECaLS: Detailed visual morphology measurements from volunteers and deep learning for 314 000 galaxies, Monthly Notices of the Royal Astronomical Society **509**, 3966 (2022), arXiv:2102.08414 [astro-ph.GA].